J. Plasma Physics (2000), *vol.* 64, *part* 4, *pp.* 507–541. Printed in the United Kingdom

Transport of energetic charged particles in a radial magnetic field. Part 1. Large-angle scattering

G. P. ZANK,[1] J. Y. LU,[1,2] W. K. M. RICE[1] and G. M. WEBB[3]

[1] Bartol Research Institute, University of Delaware, Newark, DE 19716, USA
[2] Center for Space Science and Applied Research, Chinese Academy of Sciences, Beijing, 100080, China
[3] Lunar and Planetary Laboratory, University of Arizona, Tucson, AZ 85721, USA

(Received 11 August 2000)

Abstract. A new approach, the propagating-source method, is introduced to solve the time-dependent Boltzmann equation. The method relies on the decomposition of the particle distribution function into scattered and unscattered particles. It is assumed in this paper that the particles are transported in a constant-velocity spherically expanding supersonic flow (such as the solar wind) in the presence of a radial magnetic field. Attention too has been restricted to very fast particles. The present paper addresses only large-angle scattering, which is modelled as a BGK relaxation time operator. A subsequent paper (Part 2) will apply the propagating-source method to a small-angle quasilinear scattering operator. Initially, we consider the simplest form of the BGK Boltzmann equation, which omits both adiabatic deceleration and focusing, to re-derive the well-known telegrapher equation for particle transport. However, the derivation based on the propagating-source method yields an inhomogeneous form of the telegrapher equation; a form for which the well-known problem of coherent pulse solutions is absent. Furthermore, the inhomogeneous telegrapher equation is valid for times t much smaller than the 'scattering time' τ, i.e. for times $t \ll \tau$, as well as for $t > \tau$. More complicated forms of the BGK Boltzmann equation that now include focusing and adiabatic deceleration are solved. The basic results to emerge from this new approach to solving the BGK Boltzmann equation are the following. (i) Low-order polynomial expansions can be used to investigate particle propagation and transport at arbitrarily small times in a scattering medium. (ii) The theory of characteristics for linear hyperbolic equations illuminates the role of causality in the expanded integro-differential Fokker–Planck equation. (iii) The propagating-source approach is not restricted to isotropic initial data, but instead arbitrarily anisotropic initial data can be investigated. Examples using different ring-beam distributions are presented. (iv) Finally, the numerical scheme can include both small-angle and large-angle particle scattering operators (Part 2). A detailed discussion of the results for the various Boltzmann-equation models is given. In general, it is found that particle beams that experience scattering by, for example, interplanetary fluctuations are likely to remain highly anisotropic for many scattering times. This makes the use of the diffusion approximation for charged-particle transport particularly

dangerous under many reasonable solar-wind conditions, especially in the inner heliosphere.

Dedication

This paper is dedicated to John Dougherty on the occasion of his 65th birthday.

1. Introduction

A basic problem in space physics and astrophysics is the transport of charged particles in the presence of a magnetic field that is ordered on some large scale and highly random and temporal on other smaller scales. Various approaches to the problem of particle transport in a scattering medium have been followed over the years, most notably the Chapman–Enskog expansion method, and a paper of particular interest in the context of this birthday issue of the *Journal of Plasma Physics* is one by Dougherty, Watson, and Hellberg (1967). Since the first author of the present paper has ties to the first and third of these authors, it seems particularly appropriate on this occasion to write an article on the subject of particle transport. In the solar wind, MHD turbulence, including Alfvén waves, acts to scatter solar energetic particles, anomalous and galactic cosmic rays, and pickup ions, for example. It is assumed typically that magnetic fluctuations induce small-angle scattering of the charged particles and that the scattering may be modelled by diffusion in particle pitch angle. Scattering in the solar wind is, however, unlikely to be restricted to small-angle scattering in pitch angle, since magnetic structures are frequently present in the solar wind on all scales (see e.g. Burlaga 1995), and these may be responsible for large-angle scattering. The simplest example is a sharply bent fluctuation in the magnetic field that forces a charged particle to experience mirroring. Thus, particle transport in the solar wind and other magnetically turbulent regions is likely to result from a combination of small-angle and large-angle scattering.

The purpose of this work is to investigate particle transport in the presence of both small-angle and large-angle scattering. In this first paper, we restrict our attention to large-angle scattering only. A subsequent paper (Zank et al. 2000; henceforth referred to as Part 2) will extend the techniques developed here to both small- and large-angle scattering models. Our approach is based upon Legendre-expansion techniques built around the BGK scattering operator, and is unique in that we introduce a simple approach to describing the propagation of particles for times small compared with the scattering time scale. The small-angle scattering (Part 2) is described on the basis of quasilinear theory and the large-angle scattering by the BGK relaxation-time approximation.

The transport of charged particles along a magnetic field is governed by the Fokker–Planck equation. By assuming that the charged-particle distribution function $f(\mathbf{x}, t, \mathbf{v})$ is nearly gyrotropic, the gyrophase-averaged Boltzmann equation in a stationary frame may be expressed as (Skilling 1971; Isenberg 1997)

https://doi.org/10.1017/S0022377800008709 Published online by Cambridge University Press

$$\frac{\partial f}{\partial t}+(u_i+v\mu b_i)\frac{\partial f}{\partial x_i}+\left[\frac{1-3\mu^2}{2}b_i b_j\frac{\partial u_i}{\partial x_i}-\frac{1-\mu^2}{2}\frac{\partial u_i}{\partial x_i}-\frac{\mu b_i}{v}\left(\frac{\partial u_i}{\partial t}+u_j\frac{\partial u_i}{\partial x_j}\right)\right]v\frac{\partial f}{\partial v}$$

$$+\frac{1-\mu^2}{2}\left[v\frac{\partial b_i}{\partial x_i}+\mu\frac{\partial u_i}{\partial x_i}-3\mu b_i b_j\frac{\partial u_i}{\partial x_j}-\frac{2b_i}{v}\left(\frac{\partial u_i}{\partial t}+u_j\frac{\partial u_i}{\partial x_j}\right)\right]\frac{\partial f}{\partial \mu}=\left(\frac{\delta f}{\delta t}\right)_c+S-L. \qquad (1.1)$$

In (1.1), the distribution function $f(\mathbf{x}, t, \mathbf{v}) = f(\mathbf{x}, t, \mu, v)$, where the pitch angle θ defines $\mu \equiv \mathbf{v}\cdot\mathbf{b}/\mathbf{b} = \cos\theta$, $\mathbf{b} = \mathbf{B}_0/|\mathbf{B}_0|$ is the unit vector aligned with the large-scale magnetic field $\mathbf{B}_0$, v denotes the particle speed, and $\mathbf{u}$ is the large-scale bulk flow velocity. The variables $\mathbf{x}$ and t denote the particle position and time respectively, and S and L are source and loss terms respectively. Cross-field diffusion and particle drifts are neglected in (1.1), as is energy diffusion.

The scattering operator $(\delta f/\delta t)_c$ describes particle scattering by random magnetic fluctuations, and is given either by a quasilinear pitch-angle model or by a relaxation-time model. The former may be expressed as

$$\left(\frac{\delta f}{\delta t}\right)_c = \frac{\partial}{\partial \mu}\left[Q(\mu, \tau_q)\frac{\partial f}{\partial \mu}\right], \qquad (1.2)$$

where $Q(\mu, \tau_q)$ is the particle scattering frequency (see e.g. Jokipii 1966), and is a function of pitch angle and the quasilinear small-angle scattering time τ_q. The expression (1.2) may be regarded as a collision term appropriate to small-angle scattering. The BGK Boltzmann collision operator or relaxation-time approximation,

$$\left(\frac{\delta f}{\delta t}\right)_c = \frac{\langle f\rangle - f}{\tau}, \qquad (1.3)$$

is often used instead of (1.2) (Gombosi et al. 1993; Kota 1994), and describes isotropic large-angle scattering. In (1.3), $\langle f\rangle \equiv \frac{1}{2}\int_{-1}^{1} f\, d\mu$ is the isotropic distribution function f averaged over pitch angle μ, and $\tau = \tau(\mathbf{x}, v, \mu)$ is the collision or scattering time.

Both forms of the Fokker–Planck equation, i.e. using either (1.2) or (1.3), can be reduced to a diffusion equation describing particle propagation (Jokipii 1966; Gleeson and Axford 1967; Hasselmann and Wibberenz 1970), which is inappropriate for early times (with respect to the scattering timescale) after the impulsive release of particles from a source. The non-causal or infinite signal speed implicit in the diffusion-equation description can be avoided by using instead a telegrapher equation description for the omnidirectional phase-space density (Fisk and Axford 1969; Earl 1974; Gombosi et al. 1993; Pauls and Burger 1993). However, as we discuss further below, the telegrapher-equation models do not in general describe large anisotropies at early times adequately, although they do offer some improvement over the non-causal diffusion-equation description provided that particle anisotropies are small.

Our goal in this series of papers, of which this is the first, is to develop a new quasinumerical approach to solving the Fokker–Planck equation (1.1) with either of the scattering operators (1.2) or (1.3), while drawing on the rich heritage of polynomial-expansion methods. Standard numerical approaches to the solution of the Boltzmann equation (Ng and Wong 1979; Kota et al. 1982; Ruffulo 1991; Heras et al. 1995; Kallenrode and Hatzky 1999) do not always provide a satisfactory understanding of the physics underlying particle

transport when compared with either the telegrapher or diffusion equations, and are often computationally challenging. Chalov and Fahr (1998, 1999a, b) have used a stochastic-equation reduction of the transport equation to investigate particle transport in a small-angle scattering medium. In this paper, we shall restrict our attention to large particle energies (i.e. $v \gg u$), and consider a constant flow speed u and radial magnetic field. Subject to these assumptions, (1.1) reduces to

$$\frac{\partial f}{\partial t}+\mu v\frac{\partial f}{\partial r}-\frac{1-\mu^2}{r}uv\frac{\partial f}{\partial v}+\frac{1-\mu^2}{r}v\frac{\partial f}{\partial \mu}=\left(\frac{\delta f}{\delta t}\right)_c. \tag{1.4}$$

We shall also discuss a slight complication of (1.4), which includes anisotropic large-angle scattering. The terms in (1.4) describe (neglecting the time derivative) convection, adiabatic cooling, and adiabatic focusing. The basic property that we demand of our quasinumerical approach is that it describe both the early coherent phase of particle propagation and the more isotropic diffusive transport characteristics of later times. In this paper, the collisional term of (1.4) is restricted to the BGK operator (1.3).

In developing the theoretical approach, we consider first in Sec. 2 the simplest form of (1.4), which neglects both adiabatic deceleration (third term) and focusing (fourth term) in the spherically expanding solar wind. Our reasons for considering the simplest example again (an example studied by numerous authors; e.g. Earl 1974; Gombosi et al. 1993; Federov and Shakhov 1993; Kota 1994; Webb et al. 1999, 2000) are twofold: it affords the simplest exposition of our numerical approach, and it can be related directly to the well-known telegrapher-equation model of charged-particle transport. Furthermore, the method that we shall introduce to solve the Boltzmann equation (1.4) subject to small-angle scattering will use techniques closely related to those introduced to solve the BGK form of the Boltzmann equation. In Sec. 3, we extend the simplest example discussed in Sec. 2 to include anisotropic scattering. By comparing our numerical solutions with the exact solutions of Kota (1994), we demonstrate explicitly that our numerical scheme is very accurate for low-order polynomial expansions. Section 4 considers the inclusion of focusing in the isotropic scattering model, and we conclude in Sec. 5 with a brief discussion.

The basic results to emerge from this new approach to solving the BGK Boltzmann equation are the following.

(i) Low-order polynomial expansions can be used to investigate particle propagation and transport at arbitrarily small times in a scattering medium.

(ii) The theory of characteristics for linear hyperbolic equations illuminates the role of causality in the expanded integro-differential Fokker–Planck equation.

(iii) Our approach is not restricted to isotropic initial data, but instead arbitrarily anisotropic initial data can be investigated. Examples using different ring-beam distributions are presented.

(iv) The numerical scheme can include both small-angle and large-angle particle scattering operators (Part 2).

These results are expanded upon in Sec. 5.

https://doi.org/10.1017/S0022377800008709 Published online by Cambridge University Press

2. The simplest example and the telegrapher equation

In this paper, we restrict our attention to a BGK relaxation-time scattering operator. The method that we introduce to solve the small-angle scattering operator is based on an extension of the integral formulation of the BGK operator, for which the results of Secs 2–4 are necessary.

2.1. The telegrapher equation: overview

The diffusion-equation description of charged-particle transport is not valid at early times since it is non-causal and has an infinite speed for the propagaton of disturbances. The infinite signal speed can be avoided by using instead a telegrapher-equation description,

$$\tau\frac{\partial^2\langle f\rangle}{\partial t^2}+\frac{\partial\langle f\rangle}{\partial t}-\kappa\frac{\partial^2\langle f\rangle}{\partial r^2}=0, \tag{2.1}$$

$$\kappa=\tfrac{1}{3}v^2\tau,$$

for the omnidirectional phase-space density $\langle f\rangle$ of particles with fixed speed v. The telegrapher equation (2.1) is derived by truncating the eigenfunction moment equations (Fisk and Axford 1969; Earl 1974a, b; Gombosi et al. 1993; Pauls et al. 1993) and includes the effects of particle inertia.

Analytical solutions to (2.1) are obtained easily, provided the initial data is *isotropic*. Thus, telegrapher-equation models do not describe large anisotropies in the evolving distribution at early times. Nonetheless, (2.1) is hyperbolic, admitting the forward and backward characteristic signal speeds $\pm v/\sqrt{3}$, together with dispersive-like behaviour at later times. Solutions to the telegrapher equation can be interpreted schematically as illustrated in Fig. 1.

For an impulsive source, the (analytical) solution of (2.1) shows that two leading pulses proportional to

$$\langle f\rangle\left(r-\frac{v}{\sqrt{3}}\right)+\langle f\rangle\left(r+\frac{v}{\sqrt{3}}\right)$$

propagate ahead of the diffusive wake. However, the instantaneous formation of leading pulses is evidently unphysical. As observed by Gombosi et al. (1993), early phases of particle propagation, when particles have experienced little or no scattering, must remain uniform (or 'box'-like) in the case of isotropic injection. Indeed, full solutions of the BGK Boltzmann equation underlying (2.1) do not exhibit coherent pulse-like solutions (Earl 1993; Federov and Shakhov 1993; Kota 1994; Federov et al. 1995), and the pulses of the telegrapher equation are misleading. It is now well established that coherent pulses can only appear at early times if the pitch-angle scattering is highly anisotropic (Earl 1993; Kota 1994).

In an attempt to circumvent some of the above difficulties, Gombosi et al. (1993) expanded the BGK Boltzmann equation asymptotically in a 'diffusion parameter' to obtain a higher-order modified telegrapher equation that had two signal speeds slightly different from the familiar $\pm v/\sqrt{3}$ of (2.1). Nonetheless, the modified telegrapher equation remains invalid at early times, is restricted to isotropic initial data, and, as we argue below, the modified phase speed does not capture the essential scattered-particle propagation characteristics substantially better than the original telegrapher equation. Never-

https://doi.org/10.1017/S0022377800008709 Published online by Cambridge University Press

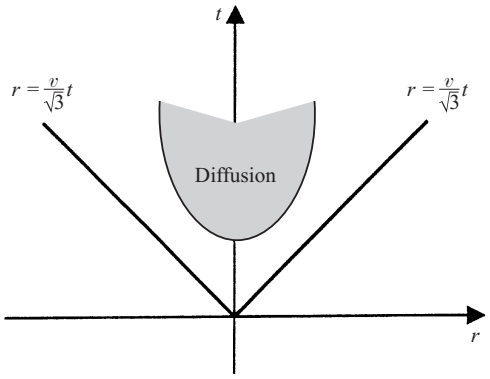

Figure 1. Schematic of the solution domain of the telegrapher equation in space–time coordinates. The characteristics $r = \pm vt/\sqrt{3}$ ensure the causal character of the solutions, bounding the regime for which solutions exist. At later times, solutions acquire a different character.

theless, for small spatial variations, the modified telegrapher equation provides slightly more accurate solutions than the standard telegrapher equation (Schwadron and Gombosi 1994).

2.2. The simplest example

In the absence of both focusing and adiabatic energy changes, the BGK Boltzmann equation (1.4) reduces to the simplest possible integro-differential equation,

$$\frac{\partial f}{\partial t} + \mu v \frac{\partial f}{\partial r} = \frac{\langle f \rangle - f}{\tau}, \tag{2.2}$$

where $f = f(r, t, \mu, v)$ is the velocity-space distribution function at position r and time t for particles of speed v and pitch-angle cosine $\mu = \cos\theta$; $\langle f \rangle \equiv \frac{1}{2}\int_{-1}^{1} f\, d\mu$ is the mean or isotropic distribution function averaged over μ, and $\tau \equiv \tau(r, \mu, v)$ is the collision time. We shall consider the Cauchy problem for (2.2) with arbitrary initial data given by

$$f(r, t = 0, \mu, v) = F(r, 0, \mu, v). \tag{2.3}$$

No restrictions are imposed on the form of the initial data, i.e. it need not be isotropic, and we shall frequently consider an initial ring-beam distribution

$$F(r, 0, \mu, v) = \frac{N(r)\delta(v - v_0)\delta(\mu - \mu_0)}{2\pi v^2}. \tag{2.4}$$

In (2.4), $N(r)$ denotes the particle number density as a function of position.

As discussed by Gombosi et al. (1993), at very early times, an initial particle distribution should propagate virtually ballistically until such time as scattering begins to modify the distribution. Thus, particle scattering may be viewed as a loss process for the unscattered streaming particles, with a decay time given by the scattering time τ. Conversely, no scattered particles exist at early times, and instead the scattered distribution grows from zero as the unscattered streaming distribution decays. Thus, initial data can be prescribed for the unscattered-particle distribution, which, as it decays, leads to the formation of a scattered-particle distribution, discussed originally by Zank

https://doi.org/10.1017/S0022377800008709 Published online by Cambridge University Press

et al. (1999). This is reminiscent of the multiple-scattering solution of the Boltzmann equation presented by Webb et al. (1999). The above comments suggest that we should split the distribution function f into an 'unscattered' part F and a 'scattered' part f^s according to the decomposition

$$f = F + f^s, \tag{2.5}$$

so that (2.2) may be expressed as

$$\frac{\partial F}{\partial t} + \mu v \frac{\partial F}{\partial r} = -\frac{F}{\tau}; \tag{2.6}$$

$$\frac{\partial f^s}{\partial t} + \mu v \frac{\partial f^s}{\partial r} + \frac{f^s}{\tau} = \frac{F_0}{\tau} + \frac{f_0}{\tau}. \tag{2.7}$$

In (2.7),

$$F_0 \equiv \frac{1}{2}\int_{-1}^{1} F\, d\mu, \qquad f_0 \equiv \frac{1}{2}\int_{-1}^{1} f^s\, d\mu.$$

Note that F can only lose particles unless an explicit source term is present. Evidently, F_0 is a source term for the scattered-particle distribution, and, unlike the prescribed initial data, is a moving source. Such a distributed source of scattered particles will eliminate the possibility of coherent pulses forming for isotropic scattering.

The solution to (2.6) with the initial data (2.3) is simply

$$F(r, t, \mu, v) = F(r - \mu v t, 0, \mu, v) e^{-t/\tau}, \tag{2.8}$$

which describes a ballistically propagating but decaying initial distribution. The corresponding source term for (2.7) is

$$F_0 = \frac{1}{2}\int_{-1}^{1} F(r - \mu v t, 0, \mu, v) e^{-t/\tau}\, d\mu. \tag{2.9}$$

To solve (2.7), we may expand f^s in an infinite series of Legendre polynomials $P_n(\mu)$:

$$f^s = \frac{1}{4\pi}\sum_{n=0}^{\infty} (2n+1) P_n(\mu) f_n(r, t, v), \tag{2.10}$$

where $f_n(r, t, v)$ is the nth harmonic of the scattered distribution function

$$\begin{aligned} f_n(r, t, v) &= \iint f^s(r, t, \mu, v) P_n(\mu)\, d\Omega \\ &= 2\pi \int_{-1}^{1} f^s(r, t, \mu, v) P_n(\mu)\, d\mu, \end{aligned} \tag{2.11}$$

$$P_0(\mu) = 1, \qquad P_1(\mu) = \mu, \qquad P_2(\mu) = \tfrac{1}{2}(3\mu^2 - 1), \qquad \ldots \quad .$$

By means of the usual recursion relation $(n+1)P_{n+1} + nP_{n-1} = (2n+1)\mu P_n$, we obtain the infinite set of partial differential equations

$$(2n+1)\frac{\partial f_n}{\partial t} + (n+1)v\frac{\partial f_{n+1}}{\partial r} + nv\frac{\partial f_{n-1}}{\partial r} + (2n+1)\frac{f_n}{\tau} = (2n+1)\frac{\delta_{n0}}{\tau}(f_0 + 4\pi F_0), \tag{2.12}$$

https://doi.org/10.1017/S0022377800008709 Published online by Cambridge University Press

where $\delta_{ij} = 0$ $(i \neq j)$ or 1 $(i = j)$.

2.3. The f_1 approximation

In (2.12), one is faced with a closure problem, which is commonly addressed by simply truncating the infinite set of equations at some arbitrary order with the hope that this does not introduce any unphysical character into the reduced model. Typically, truncations are made at the lowest order possible. For the f_1 approximation (i.e. assume $f_n = 0 \,\forall\, n \geqslant 2$), we have

$$\left.\begin{aligned} \frac{\partial f_0}{\partial t} + v\frac{\partial f_1}{\partial r} &= 4\pi\frac{F_0}{\tau} \\ \frac{\partial f_1}{\partial t} + \frac{v}{3}\frac{\partial f_0}{\partial r} &= -\frac{f_1}{\tau}, \end{aligned}\right\} \tag{2.13}$$

which can be combined to yield an inhomogeneous telegrapher equation

$$\tau\frac{\partial^2 f_0}{\partial t^2} + \frac{\partial f_0}{\partial t} - \kappa\frac{\partial^2 f_0}{\partial r^2} = 2\pi\frac{\partial F_0}{\partial t}, \tag{2.14}$$

with $\kappa = \frac{1}{3}v^2\tau$. Equations (2.13) and (2.14) admit the usual propagation speed $\pm v/\sqrt{3}$. The inhomogeneous term in (2.13) and (2.14) is the source term for the isotropic scattered component, and the initial data is only with respect to F in (2.8). The inhomogeneous telegrapher equation can be solved analytically, yielding

$$f_0(r,t,v) = e^{-t/2\tau} g_0(r,t,v), \tag{2.15}$$

$$g_0(r,t,v) = \frac{\sqrt{3}\pi}{v\tau}\int_0^t \int_{r-(v/\sqrt{3})(t-\eta)}^{r+(v/\sqrt{3})(t-\eta)} \frac{\partial F_0}{\partial t}(\xi,\eta) \times e^{-\eta/2\tau} I_0\left(\frac{1}{2}\frac{\sqrt{3}}{v\tau}\left[\frac{v^2}{3}(t-\eta)^2 - (r-\xi)^2\right]^{1/2}\right) d\xi\, d\eta,$$

where $I_0(z) = J_0(iz)$ is the modified Bessel function of order 0.

Although somewhat cumbersome, especially when one is using an explicit expression for the source term F_0, the solution (2.15) reveals several important features that distinguish the transport equation (2.14) from the standard form (2.1). The solution (2.15) for the scattered particles grows gradually from 0 at the initial time. The combined distribution $f = F + (4\pi)^{-1}(f_0 + 3\mu f_1)$ describes the evolution of the particle distribution function at all times, including $t < \tau$. Furthermore, no coherent pulses are present in the solution (2.15), and this, as discussed above, is a consequence of a moving source term. The absence of pulses can be understood schematically as illustrated in Fig. 2.

2.4. The f_n truncation

The expanded system of equations (2.12) in the f_n truncation forms a linear hyperbolic system of partial differential equations

$$\boldsymbol{\Psi}_t + v\mathbf{A}\boldsymbol{\Psi}_r = \mathbf{C}, \tag{2.16}$$

https://doi.org/10.1017/S0022377800008709 Published online by Cambridge University Press

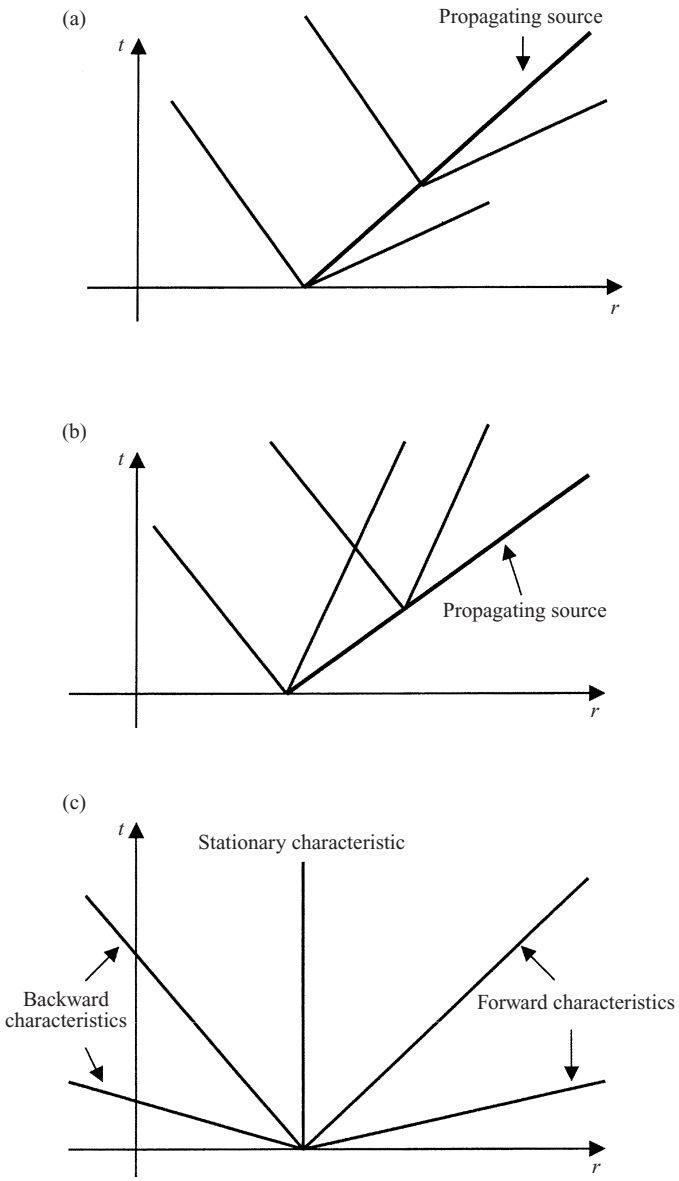

Figure 2. (a) and (b) illustrate schematically the solution to the inhomogeneous telegrapher equation (2.14). The heavy line denotes the source term corresponding to the decay of the unscattered particle distribution. The lighter 'fishbone' lines emerging from the source line are the forward and backward characteristics of newly born scattered particles. Evidently, the presence of a moving source introducing new scattered particles at later times prevents the formation of forward and backward moving coherent pulses. (a) shows a source term moving more slowly than $v/\sqrt{3}$. (b) shows a source exceeding $v/\sqrt{3}$. (c) illustrates the forward and backward stationary characteristics that arise in the f_4 truncation. See text for further discussion.

https://doi.org/10.1017/S0022377800008709 Published online by Cambridge University Press

with a (discrete) spectrum of characteristic speeds. Here $\mathbf{\Psi} = (f_0, f_1, f_2, \ldots)^{\mathrm{t}}$, t denoting transpose, $\mathbf{A}$ is the tridiagonal matrix

$$\mathbf{A} = \begin{pmatrix} 0 & 1 & 0 & 0 & 0 & \ldots & \ldots & 0 \\ \frac{1}{3} & 0 & \frac{2}{3} & 0 & 0 & \ldots & \ldots & 0 \\ 0 & \frac{2}{5} & 0 & \frac{3}{5} & 0 & \ldots & \ldots & 0 \\ 0 & 0 & \frac{3}{7} & 0 & \frac{4}{7} & \ldots & \ldots & 0 \\ \vdots & & & & & \ddots & \ddots & \vdots \\ 0 & 0 & 0 & 0 & \ldots & \dfrac{n-1}{2n-1} & 0 & \dfrac{n}{2n-1} \\ 0 & 0 & 0 & 0 & \ldots & 0 & \dfrac{n}{2n+1} & 0 \end{pmatrix}, \tag{2.17}$$

and

$$\mathbf{C} = \tau^{-1}\left(2\pi\frac{\partial F_0}{\partial t}, f_1, f_2, \ldots, f_n\right)^{\mathrm{t}}.$$

The characteristic equation $|\mathbf{A} - \lambda\mathbf{I}| = 0$ yields the $n+1$ characteristics of (2.16), all of which are distinct. When the truncation of (2.12) is even, i.e. when n is even, the number of characteristics is odd, and consists of $\frac{1}{2}n$ propagating information forward, $\frac{1}{2}n$ propagating information backward, and one that is stationary. For example, the f_2 characteristics are

$$\left(\frac{dr}{dt}\right)_{0,\,\pm} = 0, \pm\sqrt{\frac{3}{5}}v. \tag{2.18}$$

Whereas at the f_1 (telegrapher equation) level of truncation, all scattered particles propagate at $\pm v/\sqrt{3}$, the f_2 truncation is more refined, substituting $0, \pm\sqrt{\frac{3}{5}}v$ for the speeds of the scattered particles. When n is odd, the number of characteristics is even, with $\frac{1}{2}n$ propagating information forward and $\frac{1}{2}n$ backward. No stationary or zero characteristic exists for the f_n (n odd) truncation, revealing that the even and odd closures are fundamentally different. By increasing the number of equations in the truncation (i.e. increasing n), the accuracy with which information is propagated forwards and backwards is increased (see Fig. 2c). However, the odd truncation can never capture the non-propagating mode, and is therefore always intrinsically less accurate than the even expansion, even when the even truncation is of lower order.

Equations (2.16) can be solved numerically using the method of characteristics together with the analytic solution of (2.6). This approach captures the initial coherent or flash phase (Earl 1995; Federov and Shakhov, 1993; Federov et al. 1995; Ruffulo and Khumlumlert 1995) of particle transport together with the subsequent evolution into the diffusive regime. For an initial ring-beam distribution (2.4) and a localized number density $N(r) = H(r) - H(r - r_0)$ (where H is the Heaviside step function), (2.9) reduces to

$$F_0(r, t, v) = \frac{N(r - \mu_0 vt)\delta(v - v_0)}{4\pi v^2}e^{-t/\tau}. \tag{2.19}$$

By way of example, consider the f_4 truncation. This yields the five characteristics (Fig. 2c)

$$\lambda^2 = \tfrac{5}{9}(1 \pm 2\sqrt{\tfrac{2}{35}}),\ 0. \tag{2.20}$$

https://doi.org/10.1017/S0022377800008709 Published online by Cambridge University Press

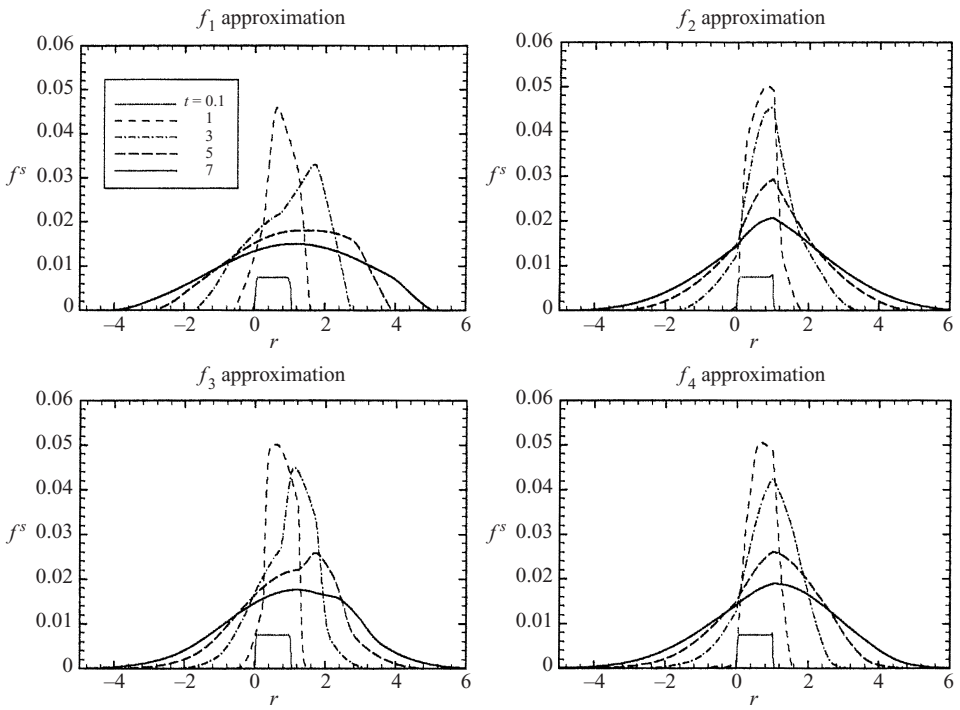

Figure 3. A comparison of solutions obtained using f_1, f_2, f_3, and f_4 truncations. The scattered distribution f^s is plotted for times ranging from early ($t = 0.1$, in normalized units) until later. The plots are along $\mu = \mu_0 = 0.25$.

For each characteristic speed λ_i, we can find the eigenvector $\boldsymbol{\xi}_i$:

$$\left.\begin{aligned} &\xi_{i1} = 1, \quad \xi_{i2} = 3\lambda_i, \quad \xi_{i3} = \tfrac{5}{2}(3\lambda_i^2 - 1), \\ &\xi_{i4} = \tfrac{7}{3}\lambda_i\,[\tfrac{5}{2}(3\lambda_i^2 - 1) - 2], \quad \xi_{i5} = \tfrac{4}{3}[\tfrac{5}{2}(3\lambda_i^2 - 1) - 2], \end{aligned}\right\} \tag{2.21}$$

for $\lambda \neq 0$. For $\lambda = 0$, we have

$$\xi_{01} = 1, \quad \xi_{02} = 0, \quad \xi_{03} = -\tfrac{5}{2}, \quad \xi_{04} = 0, \quad \xi_{05} = \tfrac{27}{8}.$$

Along each characteristic $dr/dt = \lambda_i$, the characteristic equation is

$$\sum_{j=1}^{5} \xi_{ij} \frac{df_{j-1}}{dt} = \sum_{j=1}^{5} \xi_{ij} S_j, \tag{2.22}$$

and the S_j refer to the source terms for the jth equation of (2.16).

In concluding this section, we consider three possible ring-beam distributions, these cases corresponding to $\mu_0 = 0.25$, 0.9, and 0.

Solutions to (2.2) for an initial ring-beam distribution with $\mu_0 = 0.25$ in the f_1, f_2, f_3, and f_4 truncations are illustrated in Fig. 3. The figures show only the scattered part f^s of the distribution function from an early time ($t/\tau = 0.1$) until a later time ($t/\tau = 7$) along $\mu = 0.25$. The initial beam was localized between the normalized coordinates $r = 0$ and 1. At early times, a low-amplitude flat box-like distribution of scattered particles is generated as the initial propagating beam decays. The scattered distribution, in all approximations, peaks at slightly later times ($t/\tau = 1$) while remaining very localized. The scattered-particle distribution continues to grow and spread out in time. The differences

https://doi.org/10.1017/S0022377800008709 Published online by Cambridge University Press

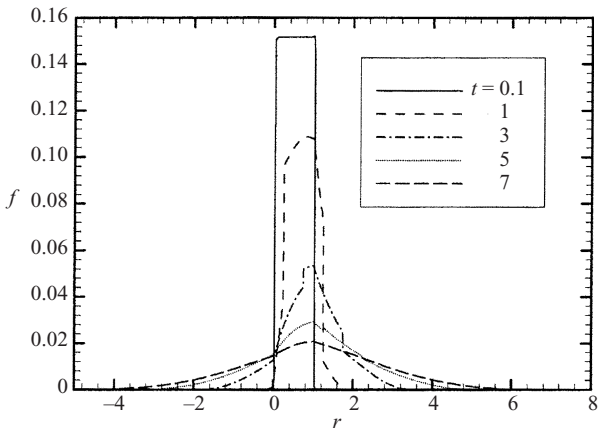

Figure 4. The total distribution $f = F + f^s$ as a function of position for times corresponding to those of Fig. 3 along $\mu = 0.25$.

between the odd and even truncations are apparent, with the odd truncations exhibiting a distinctly more spatially anisotropic distribution at later times than the comparable even cases. The f_2 truncation proves to be a good approximation to the full solution, and few significant differences exist between the f_2 and f_4 solutions. Finally, none of the solutions, including the f_1 telegrapher truncation, exhibit oppositely directed leading propagating pulses. In Fig. 4, we plot the full distribution function $f = F + f^s$ as a function of position for times corresponding to those of Fig. 3 along $\mu = 0.25$. Comparison of Figs 3 and 4 demonstrates that, at very early times, the solution f is dominated by the initial beam before relaxing at $t/\tau \geqslant 1$ into a primarily scattered distribution.

The contribution of the various harmonics to the total scattered distribution is examined in Fig. 5. Here we consider the f_2 and f_3 truncations at two times ($t = 1, t = 5$), and plot f_0, f_1, f_2, and f_3, together with f^s along $\mu = 0.25$ (equation (2.10)) as functions of position r. For both approximations, the isotropic harmonic f_0 is dominant. The f_1 harmonic is of smaller amplitude than f_0, but remains the dominant anisotropy. The harmonics f_2 and f_3 are also of small amplitude. However, the total scattered distribution f^s is not very well approximated by f_0 in shape at early times nor in amplitude at all times (compare Figs 3 and 5).

In Fig. 6, we plot the omnidirectional distribution at the f_2 truncation for the three cases $\mu_0 = 0$, 0.25, and 0.9. For small initial pitch angles, i.e. for nearly field-aligned beams, the unscattered particles move faster than the signal propagation speed. Consequently, a decaying propagating pulse is a prominent feature at early times for the scattered distribution; this is the result of a rapidly moving source of scattered particles (see Fig. 2). By contrast, when $\mu_0 = 0$, source-propagation effects are of course completely absent, and the scattered distribution simply grows from 0 at the localized source region, the initial ring-beam decays locally, and the distribution width increases symmetrically with time.

Intensity profiles for the three ring-beam cases can be plotted. In Fig. 7, we plot the total distribution f along $\mu = 0.3$ as a function of time at two spatial

https://doi.org/10.1017/S0022377800008709 Published online by Cambridge University Press

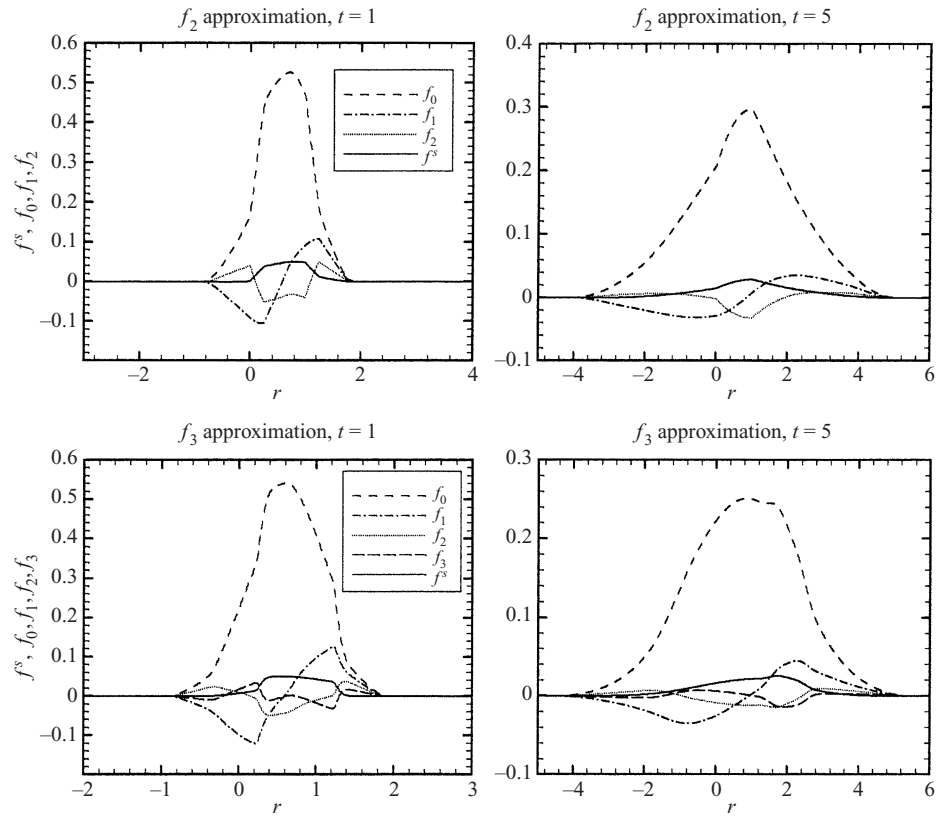

Figure 5. The contribution of the harmonics f_0, f_1, and f_2 to f^s in the f_2 approximation at times $t/\tau = 1$ and $t/\tau = 5$; and the contribution of the harmonics f_0, f_1, f_2, and f_3 to f^s in the f_3 approximation at times $t/\tau = 1$ and $t/\tau = 5$.

locations: one immediately adjacent to the source region (normalized $r = 1.3$) and the other further out ($r = 3$). Close to the source, we observe for all three cases an initial period of growth, which peaks when $t/\tau \approx 1.5$. By contrast, when observed at $r = 3$, no peak exists for either the $\mu_0 = 0$ or the $\mu_0 = 0.25$ cases, and a modest peak is present for the highly field-aligned case $\mu_0 = 0.9$. At $r = 3$, the gradient of the initial growth is inversely proportional to μ_0, with the smallest initial pitch angle yielding the longest growth time in intensity and the largest yielding the shortest. For both observation locations, the intensity decays monotonically with time. Finally, intensity profiles for the first-order anisotropy f_1 are plotted in Fig. 8, and these are quite similar in character to those of Fig. 7.

Before concluding this section, we discuss briefly the differences in propagation characteristics for particle species of different rigidities. Such differences are incorporated easily into our simple model by changing the value of the scattering parameter τ. From quasilinear theory, the parallel mean free path is well approximated by

$$\lambda_\parallel = \lambda_{\parallel 0}\left(\frac{R}{R_0}\right)^{1/3}, \tag{2.23}$$

https://doi.org/10.1017/S0022377800008709 Published online by Cambridge University Press

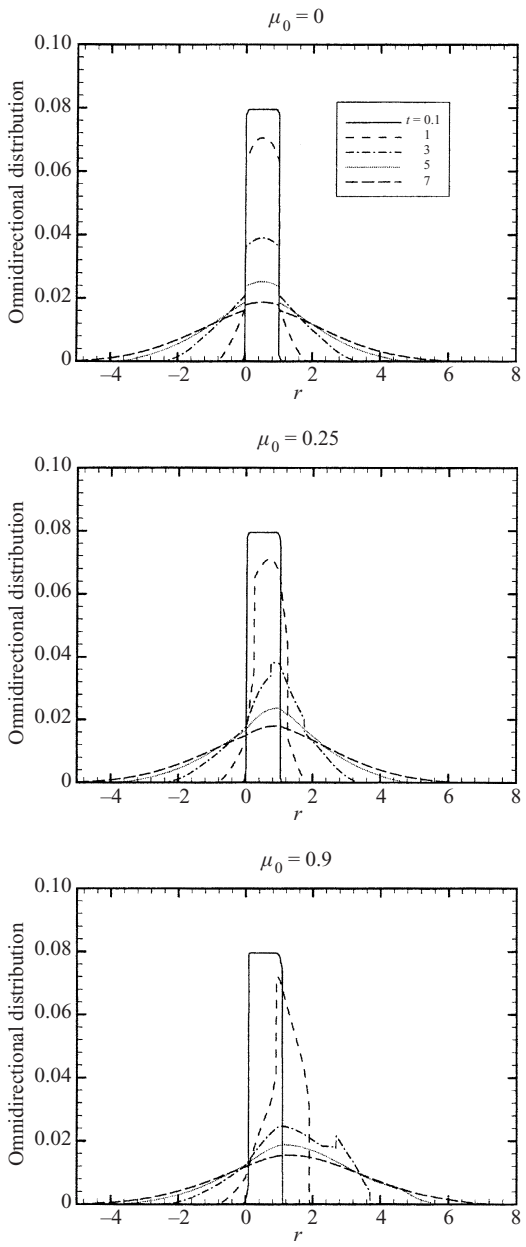

Figure 6. The influence of μ_0 (the initial pitch angle of a ring-beam distribution) on the omnidirectional distribution $\langle f \rangle$ plotted as a function of position for a range of times t/τ $(= 0.1, 1, 3, 5, 7)$.

(see equation (4) in Zank et al. 1998), where $R \equiv pc/Ze$ denotes the particle rigidity (p is the momentum, c the speed of light, and Ze the charge). Thus

$$\frac{\tau}{\tau_0} = \frac{\lambda_\parallel / v}{\lambda_{\parallel 0}/v_0} = \left(\frac{m/Z}{m_0/Z_0}\right)^{1/3}$$

for particles of equal velocity but possibly different mass and charge. The

https://doi.org/10.1017/S0022377800008709 Published online by Cambridge University Press

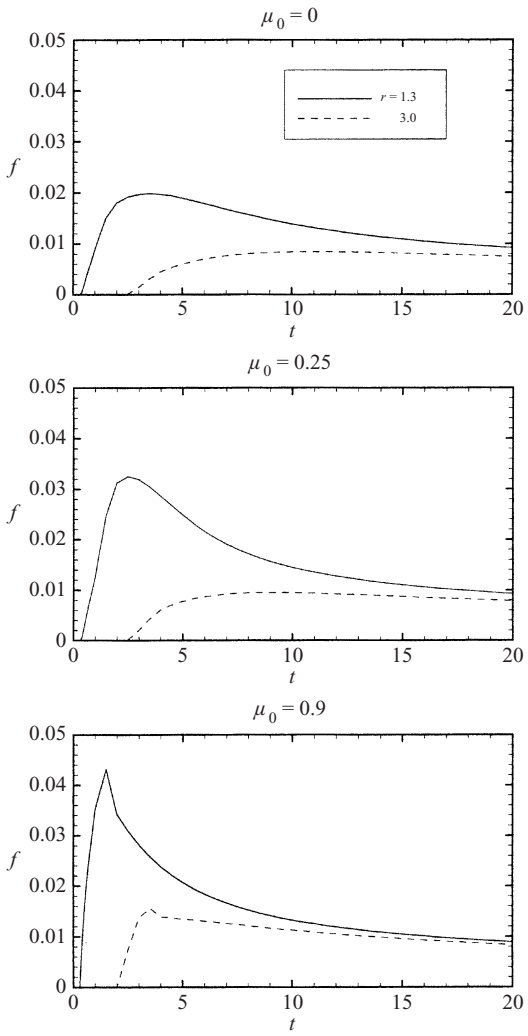

Figure 7. A plot, corresponding to Fig. 6, of the distribution function f as a function of time for $\mu = 0.3$ at two spatial locations, $r = 1.3$ and $r = 3$.

scattering time τ_0 may therefore be used as a reference to compute the propagation characteristics of particles of different rigidities. Inspection of equation (4) of Zank et al. (1998) also shows that the radially evolving turbulent magnetic fluctuations responsible for scattering the particles, i.e. the evolution in the intensity of solar-wind turbulence, can be incorporated in the radial dependence of τ. In Fig. 9, we plot intensity profiles corresponding to particles of different rigidities. In the previous calculation, $\tau/\tau_0 = 1$ corresponds to protons. Here, $\tau/\tau_0 = 2^{4/3}$ corresponds to singly charged oxygen ions with the same velocity as the protons. Comparison of Figs 7, 8, and 9 reveals a number of differences in the propagation characteristics of ions of different rigidities, particularly the smaller anisotropy exhibited by the O^+ ions.

https://doi.org/10.1017/S0022377800008709 Published online by Cambridge University Press

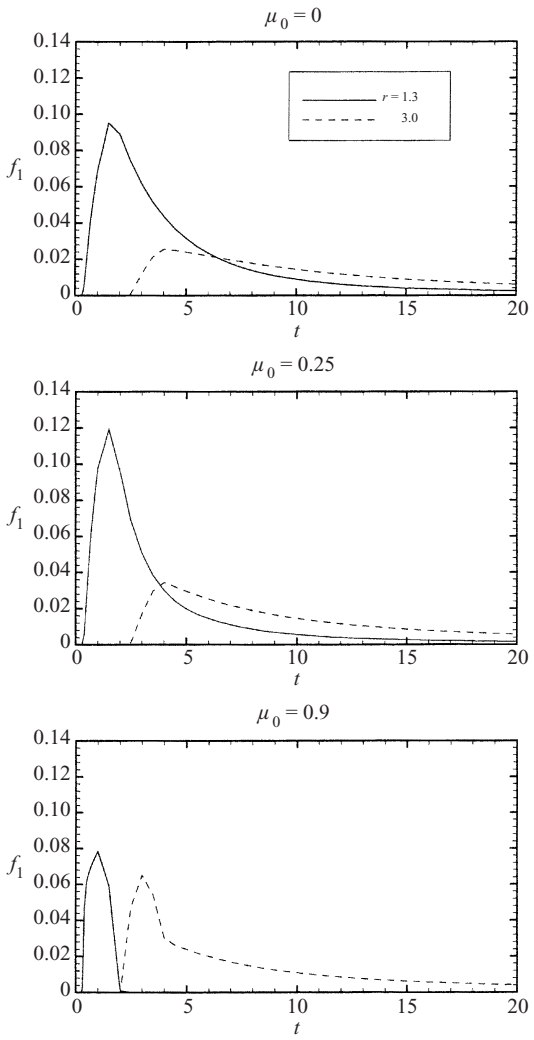

Figure 8. A plot corresponding to Fig. 7, but now plotting the first-order anisotropy f_1 as a function of time at two spatial locations, $r = 1.3$ and $r = 3$.

3. Role of anisotropic scattering

Before addressing the focusing and adiabatic deceleration terms in the BGK Boltzmann equation (1.4), we consider a slightly more complicated scattering operator than (1.3). This will also serve to introduce our approach to solving (1.4) in the presence of the small-angle scattering operator (1.2). In Sec. 2, we assumed that particles scattered from the initial beam could populate any part of the shell in velocity space. Scattering, however, is more likely to begin populating that hemisphere of the shell in which the ring beam was found initially. Furthermore, it is often thought that pitch-angle scattering of charged particles is inhibited though 90° (see e.g. Earl 1974; 1993). Observations of pickup ions (Fisk et al. 1997; Gloeckler and Geiss 1998) show anisotropic velocity distributions, which have been modelled (Isenberg 1997; Schwadron

https://doi.org/10.1017/S0022377800008709 Published online by Cambridge University Press

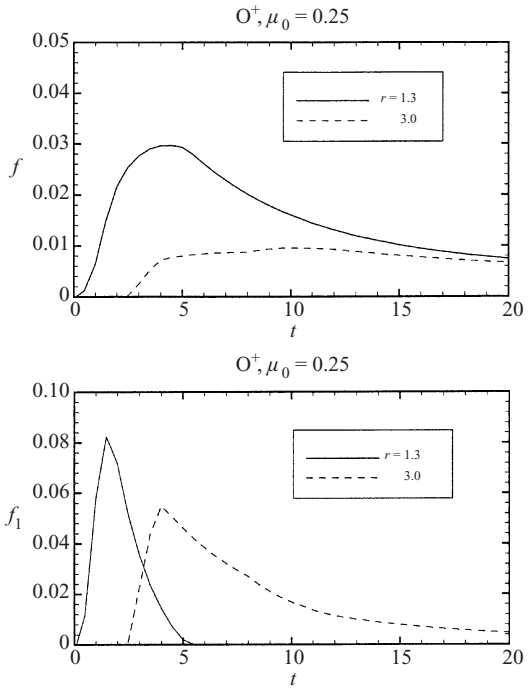

Figure 9. Plots of the distribution function f along $\mu = 0.3$ and the first-order anisotropy f_1 for O^+ ions ($t/\tau_0 = 2^{4/3}$).

1998) under the assumption that scattering from one hemisphere to the other proceeds much more slowly than scattering within each hemisphere.

One way to accommodate the more gradual and anisotropic scattering of an initial beam distribution is to introduce two scattering time scales τ_1 and τ_2. In the $\mu < 0$ and $\mu > 0$ hemispheres of velocity space, particle scattering is assumed to be isotropic and to occur at the rate τ_1^{-1}. Particle scattering from one hemisphere to another proceeds at the slower rate τ_2^{-1}. Thus, $\mu = 0$ is singular in the sense that scattering through 90° is slow. Following Kota (1994), we adopt a modified relaxation-time model analogous to (1.3) and introduce the half-range expansion $f^{\pm}$ corresponding to particles populating either the forward ($\mu > 0$) or backward ($\mu < 0$) hemispheres. Schwadron (1998) introduced a related model in his modelling of solar-wind pickup ion propagation. Accordingly, we may generalize (2.2) as

$$\frac{\partial f^-}{\partial t} + \mu v \frac{\partial f^-}{\partial r} = \frac{\langle f^- \rangle - f^-}{\tau_1} + \frac{\langle f^+ \rangle - f^-}{\tau_2} \qquad (\mu < 0), \tag{3.1}$$

$$\frac{\partial f^+}{\partial t} + \mu v \frac{\partial f^+}{\partial r} = \frac{\langle f^+ \rangle - f^+}{\tau_1} + \frac{\langle f^- \rangle - f^+}{\tau_2} \qquad (\mu > 0), \tag{3.2}$$

where

$$\langle f^- \rangle = \int_{-1}^{0} f^- \, d\mu, \qquad \langle f^+ \rangle = \int_{0}^{1} f^+ \, d\mu.$$

If $\tau_1 = \tau_2$ then the isotropic scattering model (2.2) is recovered.

https://doi.org/10.1017/S0022377800008709 Published online by Cambridge University Press

As in Sec. 2, we separate the distribution functions $f^{\pm}$ into scattered and unscattered particle distributions, i.e.

$$f^{\pm} = F^{\pm}(r,t,\mu,v)+f^{s\pm}(r,t,\mu,v). \tag{3.3}$$

Thus, rearranging (3.1) yields

$$\frac{\partial F^-}{\partial t}+\mu v\frac{\partial F^-}{\partial r} = -\frac{F^-}{\tau_1}-\frac{F^-}{\tau_2} \equiv -\frac{F^-}{\bar{\tau}}, \tag{3.4}$$

$$\frac{\partial f^{s-}}{\partial t}+\mu v\frac{\partial f^{s-}}{\partial r} = \frac{F_0^-}{\tau_1}+\frac{F_0^+}{\tau_2}+\frac{f_0^- - f^{s-}}{\tau_1}+\frac{f_0^+ - f^{s-}}{\tau_2}, \tag{3.5}$$

where

$$\bar{\tau} \equiv \frac{\tau_1\tau_2}{\tau_1+\tau_2}.$$

Similarly, for $\mu > 0$, (3.2) becomes

$$\frac{\partial F^+}{\partial t}+\mu v\frac{\partial F^+}{\partial r} = -\frac{F^+}{\bar{\tau}}, \tag{3.6}$$

$$\frac{\partial f^{s+}}{\partial t}+\mu v\frac{\partial f^{s+}}{\partial r} = \frac{F_0^+}{\tau_1}+\frac{F_0^-}{\tau_2}+\frac{f_0^+ - f^{s+}}{\tau_1}+\frac{f_0^- - f^{s+}}{\tau_2}. \tag{3.7}$$

In (3.5) and (3.7),

$$F_0^- = \int_{-1}^{0} F^- d\mu, \qquad F_0^+ = \int_0^1 F^+ d\mu.$$

The solution of (3.4) and (3.6) for the unscattered decaying-beam particles is simply

$$F^{\pm}(r,t,\mu,v) = F^{\pm}(r-\mu v t,0,\mu,v)e^{-t/\bar{\tau}}, \tag{3.8}$$

where $F^{\pm}(r,0,\mu,v)$ is the initial distribution.

To solve for the scattered particle distributions from (3.5) and (3.7), we again expand $f^{\pm}$ in terms of Legendre polynomials, but this time using a half-range expansion. Thus,

$$f^{\pm}(r,t,\mu,v) = \sum_{n=0}^{\infty}(2n+1)P_n(2\mu \mp 1)f_n(r,t,v),$$

$$f_n^+ = \int_0^1 P_n(2\mu-1)f(r,t,\mu,v)\,d\mu,$$

$$f_n^- = \int_{-1}^0 P_n(2\mu+1)f(r,t,\mu,v)\,d\mu.$$

This then yields a coupled infinite set of partial differential equations in the forward and backward harmonics $f_n^{\pm}$:

$$(2n+1)\frac{\partial f_n^{\mp}}{\partial t}+\frac{n+1}{2}v\frac{\partial f_{n+1}^{\mp}}{\partial r}+\frac{n}{2}v\frac{\partial f_{n-1}^{\mp}}{\partial r}\mp\frac{2n+1}{2}v\frac{\partial f_n^{\mp}}{\partial r}+(2n+1)\frac{f_n^{\mp}}{\bar{\tau}}$$

$$= (2n+1)\delta_{n0}\left(\frac{f_0^{\mp}+F_0^{\mp}}{\tau_1}+\frac{f_0^{\pm}+F_0^{\pm}}{\tau_2}\right). \tag{3.9}$$

https://doi.org/10.1017/S0022377800008709 Published online by Cambridge University Press

As in Sec. 2, we shall address the closure of (3.9) by truncating. In this case, we consider the f_1 and f_2 approximations. The f_1 truncation may be expressed as

$$\mathbf{\Psi}_t + v\mathbf{A}\mathbf{\Psi}_r = \mathbf{C}, \tag{3.10}$$

where $\mathbf{\Psi} \equiv (f_0^-, f_0^+, f_1^-, f_1^+)^{\mathrm{t}}$ and

$$\mathbf{A} = \begin{pmatrix} -\frac{1}{2} & 0 & \frac{1}{2} & 0 \\ \frac{1}{2\cdot 3} & 0 & -\frac{1}{2} & 0 \\ 0 & \frac{1}{2\cdot 3} & 0 & \frac{1}{2} \end{pmatrix}, \tag{3.11a}$$

$$\mathbf{C} = \begin{pmatrix} \frac{f_0^+ - f_0^-}{\tau_2} + \frac{F_0^-}{\tau_1} + \frac{F_0^+}{\tau_2} \\ \frac{f_0^- - f_0^+}{\tau_2} + \frac{F_0^+}{\tau_1} + \frac{F_0^-}{\tau_2} \\ -\frac{f_1^-}{\bar{\tau}} \\ -\frac{f_1^+}{\bar{\tau}} \end{pmatrix}, \tag{3.11b}$$

which is again a simple linear hyperbolic system of partial differential equations. The f_1 reduction admits four phase speeds

$$\lambda_{\pm}^{+} = \tfrac{1}{2}v(1 \pm \sqrt{\tfrac{1}{3}}), \tag{3.12}$$

$$\lambda_{\pm}^{-} = -\tfrac{1}{2}v(1 \pm \sqrt{\tfrac{1}{3}}). \tag{3.13}$$

Thus, the f_1 reduction gives all forward-moving particles the speed (3.12) and all backward-moving particles the speed (3.13).

We note in passing that an 'anisotropic' diffusion reduction of (3.10) can be made by assuming that gradients in $f_1^{\pm}$ are small. This implies that

$$f_1^{\pm} \approx -\frac{v}{6}\frac{\tau_1\tau_2}{\tau_1+\tau_2}\frac{\partial f_0^{\pm}}{\partial r},$$

from which one obtains the coupled diffusion transport equations

$$\frac{\partial f_0^-}{\partial t} - \frac{v}{2}\frac{\partial f_0^-}{\partial r} + \frac{f_0^- - f_0^+}{\tau_2} = \frac{v^2}{12}\frac{\tau_1\tau_2}{\tau_1+\tau_2}\frac{\partial^2 f_0^-}{\partial r^2} + \frac{F_0^-}{\tau_1} + \frac{F_0^+}{\tau_2}, \tag{3.14}$$

$$\frac{\partial f_0^+}{\partial t} + \frac{v}{2}\frac{\partial f_0^+}{\partial r} + \frac{f_0^+ - f_0^-}{\tau_2} = \frac{v^2}{12}\frac{\tau_1\tau_2}{\tau_1+\tau_2}\frac{\partial^2 f_0^+}{\partial r^2} + \frac{F_0^+}{\tau_1} + \frac{F_0^-}{\tau_2}. \tag{3.15}$$

The slow scattering time τ_2 through 90° acts as a coupling coefficient, and the spatial diffusion coefficient is an 'inverse' function of the isotropic and anisotropic scattering time scales ($\kappa^{-1} \propto \tau_1^{-1} + \tau_2^{-1}$).

https://doi.org/10.1017/S0022377800008709 Published online by Cambridge University Press

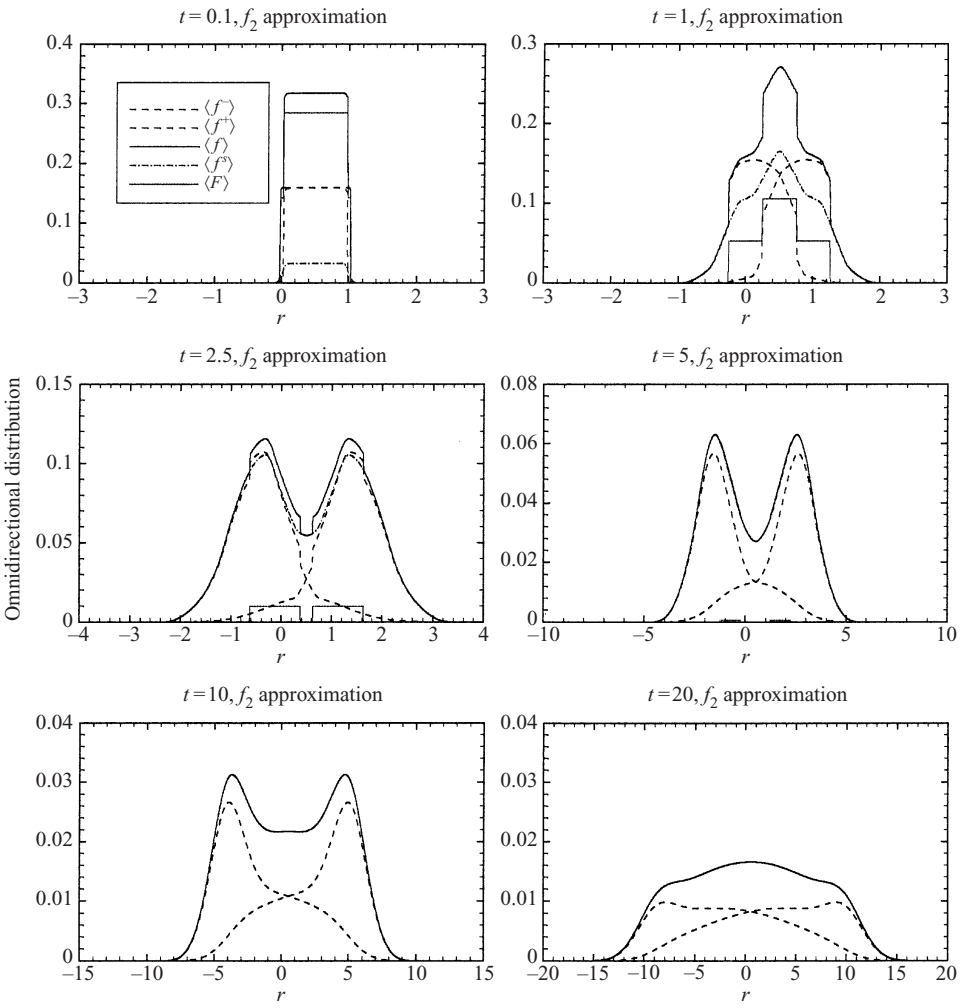

Figure 10. A sequence-in-time plot ($t = 0.1$, 1, 2.5, 5, 10, 20) showing the evolution of a pair of oppositely propagating beams. The omnidirectional distribution function $\langle f \rangle$, the scattered distribution $\langle f^s \rangle$, the beam $\langle F \rangle$, and the forward- and backward-propagating distributions $\langle f^{\pm} \rangle$ are all plotted. An f_2 approximation is used, and all times are normalized to the scattering time $\bar{\tau}$. The scattering was assumed to be highly anisotropic, with $\tau_2/\tau_1 = 10$.

For completeness, since it is discussed in the results below, the f_2 truncation is given by

$$\frac{\partial f_0^{\pm}}{\partial t} \pm \frac{v}{2}\frac{\partial f_0^{\pm}}{\partial r} + \frac{v}{2}\frac{\partial f_1^{\pm}}{\partial r} + \frac{f_0^{\pm} - f_0^{\mp}}{\tau_2} = \frac{F_0^{\pm}}{\tau_1} + \frac{F_0^{\mp}}{\tau_2}, \tag{3.16}$$

$$\frac{\partial f_1^{\pm}}{\partial t} \pm \frac{v}{2}\frac{\partial f_1^{\pm}}{\partial r} + \frac{v}{3}\frac{\partial f_2^{\pm}}{\partial r} + \frac{v}{6}\frac{\partial f_0^{\pm}}{\partial r} = -\frac{f_1^{\pm}}{\bar{\tau}}, \tag{3.17}$$

$$\frac{\partial f_2^{\pm}}{\partial t} \pm \frac{v}{2}\frac{\partial f_2^{\pm}}{\partial r} + \frac{v}{5}\frac{\partial f_1^{\pm}}{\partial r} = -\frac{f_2^{\pm}}{\bar{\tau}}. \tag{3.18}$$

https://doi.org/10.1017/S0022377800008709 Published online by Cambridge University Press

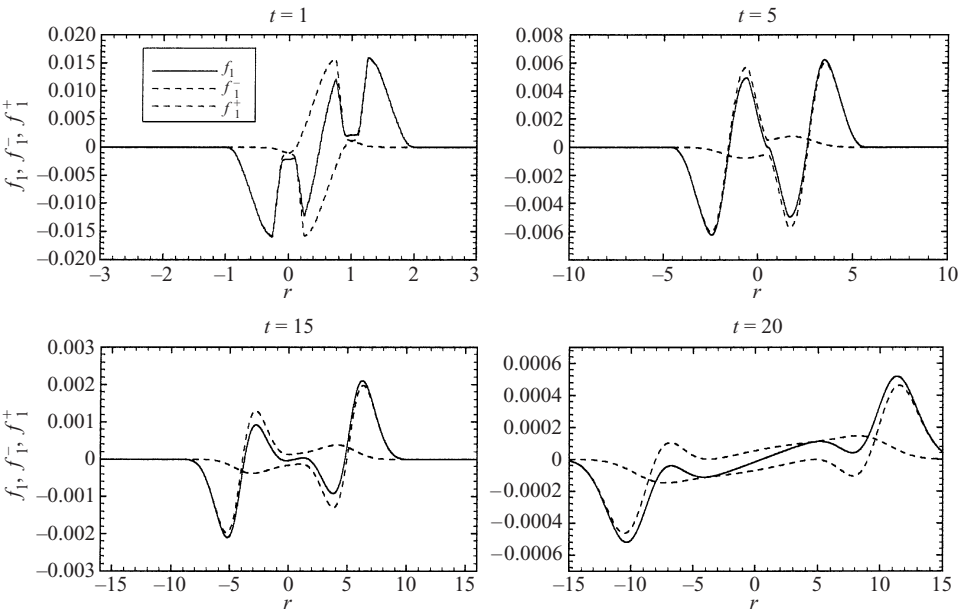

Figure 11. A time sequence ($t = 1$, 5, 10, 15, 20, 30) of the anisotropies f_1 and $f_1^{\pm}$ corresponding to Fig. 10.

The system of hyperbolic equations (3.16)–(3.18) admits six characteristic speeds: three forward and three backward modes,

$$\lambda_{\pm}^{\pm} = \pm\tfrac{1}{2}v(1 \pm \sqrt{\tfrac{3}{5}}), \qquad \lambda_{\pm} = \pm\tfrac{1}{2}v. \tag{3.19}$$

Unlike the isotropic-scattering model of Sec. 2, no fundamentally different characteristic speeds are introduced in going from an odd to an even truncation. Instead, the decomposition into signal speeds becomes increasingly refined as the order of the truncation increases.

For two initial beam distributions propagating in opposite directions ($\mu_0 = \pm 0.25$) and $\tau_2/\tau_1 = 10$ (i.e. highly anisotropic scattering), we illustrate in Fig. 10 the evolution of the omnidirectional distribution using an f_2 approximation. Such an oppositely propagating pair of beams may arise from a reconnection event, for example. The full distribution $\langle f \rangle$ (scattered and unscattered particles) is plotted in Fig. 10, together with the decomposition into forward- and backward-hemisphere particles, and scattered and unscattered particles. At early times, the evolving distribution is dominated by the ring beam. Persistent oppositely propagating coherent pulses appear at about $t/\tau = 1.5$ (in normalized units). The pulses are long-lived, surviving for more than 10 scattering times τ_0, before merging to form a broad distribution after $t/\tau = 15$. The solutions presented in Fig. 10 are virtually identical to the exact analytical solutions derived by Kota (1994; see his Fig. 4), illustrating that the low-order expansion is in fact highly accurate. Figure 11 shows the corresponding f_1 anisotropy, which maintains a relatively small amplitude. In Fig. 12, we illustrate an example of weakly anisotropic scattering for which $\tau_2/\tau_1 = 2$. Two small pulses can be seen at about $t = 2.5$, but they are short-lived and not

https://doi.org/10.1017/S0022377800008709 Published online by Cambridge University Press

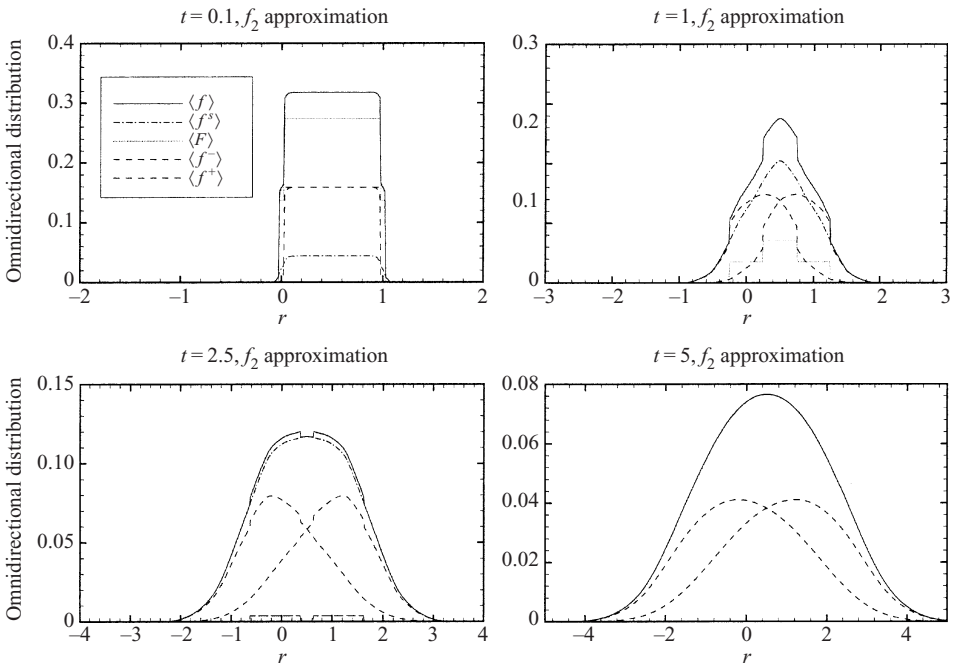

Figure 12. Like Fig. 10, a sequence-in-time plot ($t = 0.1$, 1, 2.5, 5) showing the evolution of a pair of oppositely propagating beams. The scattering is assumed to be only moderately anisotropic, with $\tau_2/\tau_1 = 2$.

obvious. Evidently, when the rate of pitch-angle scattering through 90° is small, particles in one hemisphere tend to remain bunched and persistently anisotropic. This behaviour, it has been suggested, is responsible for the long mean free paths and anisotropic distributions of interstellar pickup ions observed in quasiradial regions of the solar wind (Fisk et al. 1997; Isenberg 1997; Schwadron 1998; Lu and Zank 2000).

4. Inclusion of focusing and adiabatic deceleration

In this section, we return to the isotropic Boltzmann equation (1.4), but continue to restrict our attention to large-angle scattering.

4.1. Focusing only

In the absence of the adiabatic term, (1.4) reduces to the coupled system of equations

$$\frac{\partial F}{\partial t} + \mu v \frac{\partial F}{\partial r} + \frac{1-\mu^2}{r} v \frac{\partial F}{\partial \mu} = -\frac{F}{\tau}, \tag{4.1}$$

$$\frac{\partial f^s}{\partial t} + \mu v \frac{\partial f^s}{\partial r} + \frac{1-\mu^2}{r} v \frac{\partial f^s}{\partial \mu} = \frac{f_0 - f^s}{\tau} + \frac{F_0}{\tau}. \tag{4.2}$$

after introducing the decomposition $f = F + f^s$ as before. Our reason for concentrating on focusing here is because the initial unscattered distribution

https://doi.org/10.1017/S0022377800008709 Published online by Cambridge University Press

will become increasingly beamed in time as it propagates (and may also experience mirroring if particles propagate into the convergent radial magnetic field). Thus, the source term F_0 in (4.2) has to reflect the variation of F in pitch angle with position and time. The solution to (4.1) is obtained easily by means of characteristics for an initial distribution $F(r, t=0, \mu, v) = F(r_0, \mu_0, v)$. The analytical solution for the unscattered particles at time t is

$$r = [(\mu_0 r_0 + vt)^2 + r_0^2(1-\mu_0^2)]^{1/2}, \tag{4.3}$$

$$\mu = \left[1 - \left(\frac{r_0}{r}\right)^2 (1-\mu_0^2)\right]^{1/2}, \tag{4.4}$$

$$F(r, t, \mu, v) = F(r_0, 0, \mu_0, v) e^{-t/\tau}, \tag{4.5}$$

after using the invariants $r \sin\theta = \text{const}$ and $\mu r = \mu_0 r_0 + vt$.

Equation (4.2) is expanded as before using the Legendre polynomials (2.10)–(2.11), to obtain the infinite set of partial differential equations (now also using the recursion relation $(1-\mu^2)P'_n = nP_{n-1} - n\mu P_n$, where the prime denotes differentiation)

$$(2n+1)\frac{\partial f_n}{\partial t} + (n+1)v\frac{\partial f_{n+1}}{\partial r} + nv\frac{\partial f_{n-1}}{\partial r} + (n+2)(n+1)\frac{v}{r}f_{n+1} - n(n-1)\frac{v}{r}f_{n-1}$$

$$+ (2n+1)\frac{f_n}{\tau} = (2n+1)\frac{\delta_{n0}}{\tau}(f_0 + F_0). \tag{4.6}$$

The f_1 approximation reduces to

$$\frac{\partial f_0}{\partial t} + \frac{1}{r^2}\frac{\partial}{\partial r}(vr^2 f_1) = \frac{F_0}{\tau}, \tag{4.7}$$

$$\frac{\partial f_1}{\partial t} + \frac{v}{3}\frac{\partial f_0}{\partial r} = -\frac{f_1}{\tau}, \tag{4.8}$$

which yields, as expected, the characteristic speeds $\pm v/\sqrt{3}$ as before. The modified form of the telegrapher equation (2.14) now becomes

$$\tau\frac{\partial^2 f_0}{\partial t^2} + \frac{\partial f_0}{\partial t} - \frac{1}{r^2}\frac{\partial}{\partial r}\left(r^2\frac{v^2\tau}{3}\frac{\partial f_0}{\partial r}\right) = \frac{F_0}{\tau} + \frac{\partial F_0}{\partial t}. \tag{4.9}$$

The basic changes to the telegrapher equation (2.14) are a slightly more complicated 'moving-source' time operator for F_0, and the addition of an f_1 source term. Since focusing enhances the anisotropy, it provides an effective source term for the streaming anisotropy f_1, which can be seen by deriving the equivalent transport equation for f_1.

The f_2 (and high-order) approximation is clearly related to its non-focusing counterpart, with only the addition of a source term due to adiabatic focusing. Obviously, the characteristics remain unchanged, and the even truncations are more accurate than the odd because of the presence of the non-propagating mode.

https://doi.org/10.1017/S0022377800008709 Published online by Cambridge University Press

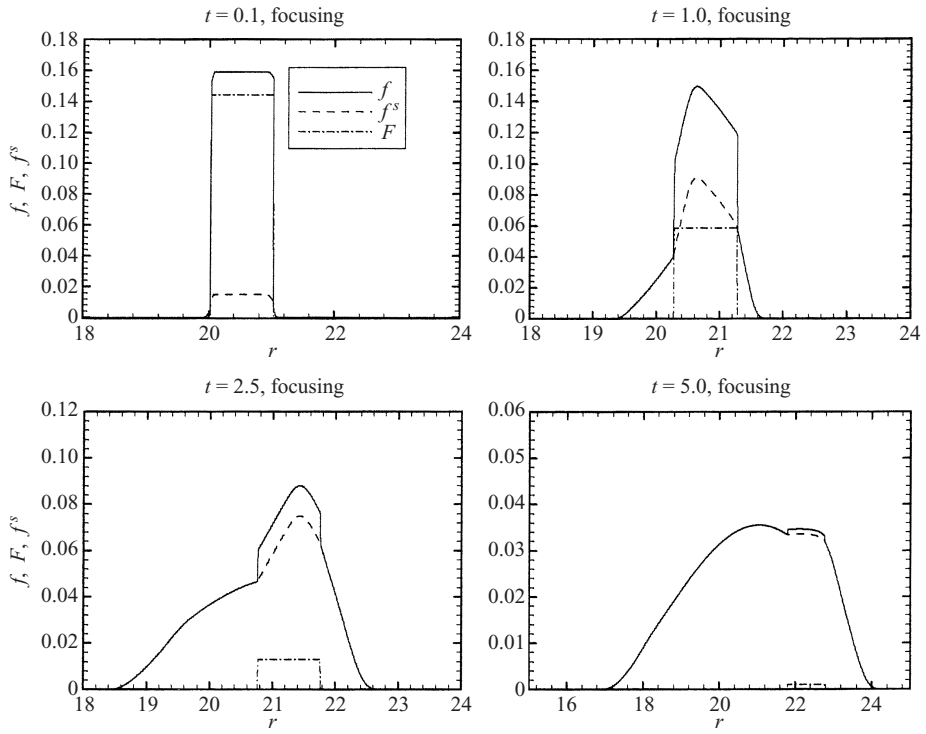

Figure 13. A time sequence of a ring beam evolving in a radial magnetic field ($t = 0.1$, 1, 2.5, 5) using the f_1 approximation. Here $\mu = \mu_0 = 0.25$. The full distribution f, the scattered distribution f^s, and the beam F are plotted separately.

Before discussing the inclusion of adiabatic deceleration in the Boltzmann equation (1.4), let us describe some results. In Fig. 13, we use the f_1 approximation to follow the radial and temporal evolution of the distribution function f from an initial ring beam with pitch angle $\mu_0 = 0.25$ localized in the (normalized) region $r \in [20, 21]$ initially. Figure 13 consists of four panels for (normalized) times ranging from $t = 0.1$ to $t = 5$. Three distributions are plotted in each panel: the full distribution function f, the scattered distribution f^s, and the unscattered distribution F. The plots are for a given value of μ ($= 0.25$). At early times, $t = 0.1$, the particles propagate ballistically. At later times, the ballistic contribution is less important, but it does distort the spatial distribution until relatively late times ($t = 5$). The inclusion of the non-propagating characteristic, i.e. the use of an even truncation, changes the results derived from the f_1 approximation quite significantly at later times, as illustrated in Fig. 14. For Fig. 14, we have used an f_4 approximation and have again plotted the three distributions f, f^s, and F. As before, the differences between the odd and even truncations are significant. Comparing the f_4 approximation (Fig. 14) with those in Fig. 3, we observe a larger asymmetry in the spatial distribution of the former, which has virtually disappeared by $t/\tau \approx 7$ and beyond. We may also plot the distribution function f as a function of pitch angle for different times and locations (Fig. 15). At later times, the particle distribution at $r = 15$ (i.e. at smaller heliocentric distances than their region of release) is shown as a function of pitch angle in the top panel. Not

https://doi.org/10.1017/S0022377800008709 Published online by Cambridge University Press

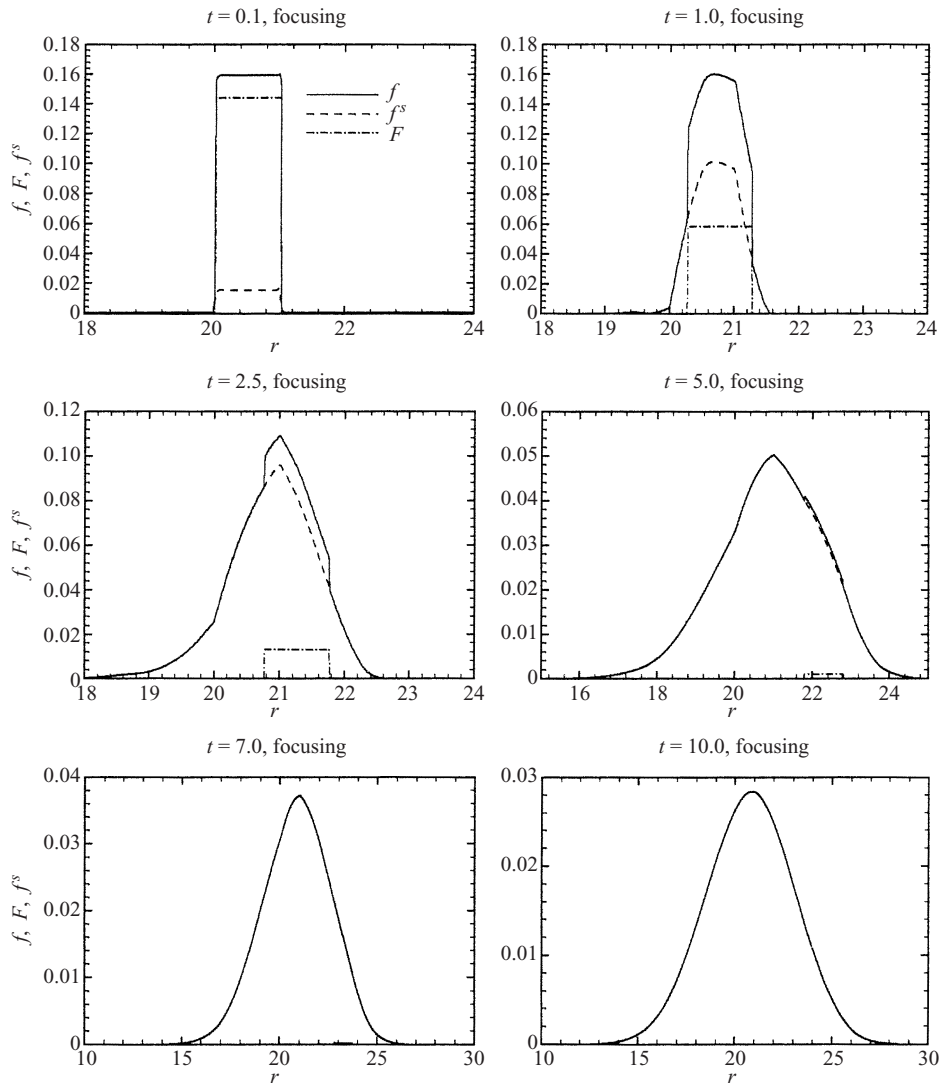

Figure 14. As Fig. 13, but now using an f_4 approximation.

surprisingly, the distribution is highly skewed towards $\mu = -1$, since only those particles scattered out of the initial ring beam ($\mu_0 = 0.25$) into a direction almost radially inward can propagate to this distance. With increasing time, more particles arrive at (normalized) $r = 15$, but the distribution remains highly anisotropic even though the distribution at $t/\tau = 10$ is now fully scattered. At their point of release, $r = 20$, the evolution in the pitch-angle distribution is from highly anisotropic at small times ($t/\tau = 1.5$) to almost completely isotropic at late times ($t/\tau = 10$). At early times, only those particles scattered into moderately negative pitch angles (≈ -0.7) have sufficient time to propagate back to $r = 20$. At large distances, $r = 25$, it is only those particles scattered into moderately large pitch angles (> 0.5) that propagate this far. Evidently, for an observer located at some radial position, the arrival of

https://doi.org/10.1017/S0022377800008709 Published online by Cambridge University Press

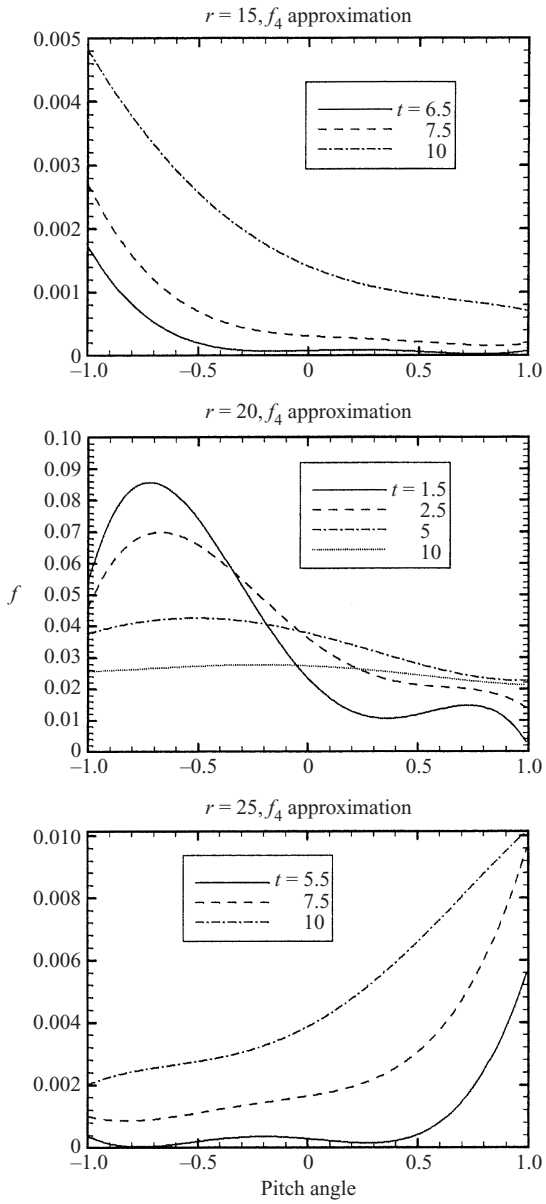

Figure 15. Plots of the full distribution function f as a function of pitch angle μ at different spatial locations ($r = 15$, 20, 25) and times for the ring-beam evolution corresponding to Fig. 14.

particles is highly pitch-angle dependent. In Fig. 16(a), we show in colour a two-dimensional intensity plot of pitch angle as a function of time t/τ for two given locations. At greater distances, focusing and scattering produces highly anisotropic pitch angle distributions. A related plot is given in Fig. 16(b), which shows an intensity plot of pitch angle as a function of position r for two different times.

https://doi.org/10.1017/S0022377800008709 Published online by Cambridge University Press

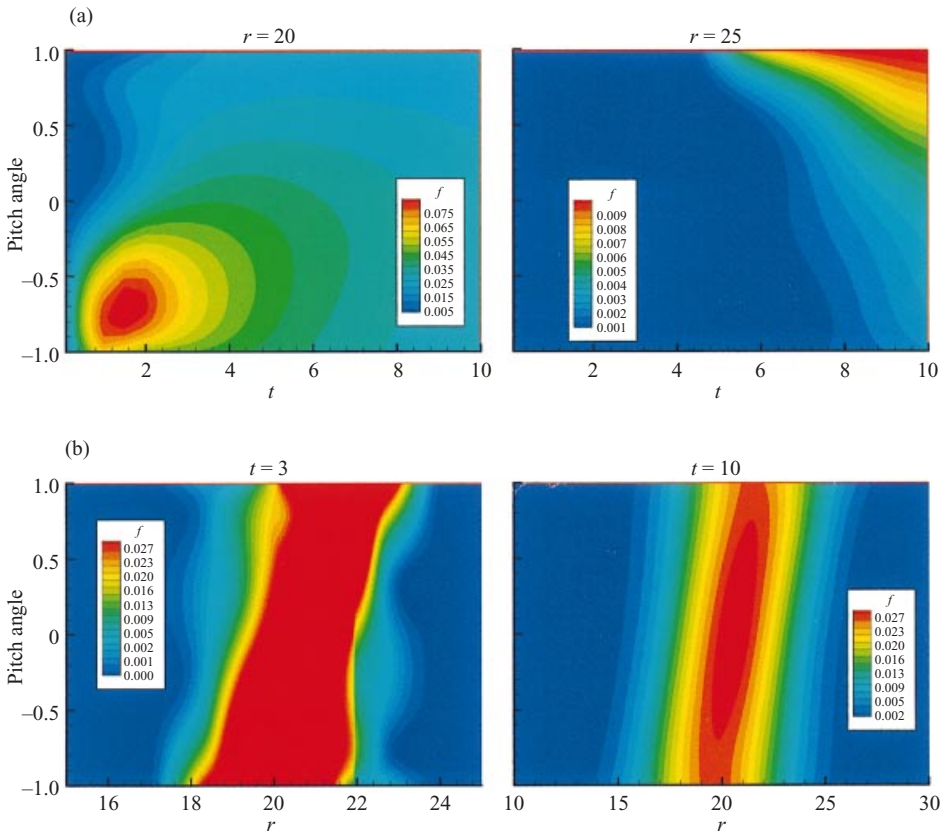

Figure 16. Colour plots of pitch angle μ: (a) as a function of time t at two fixed spatial locations, $r = 20$ and $r = 25$; (b) as a function of position r at times $t = 3$ and $t = 10$. The colour denotes the total distribution f.

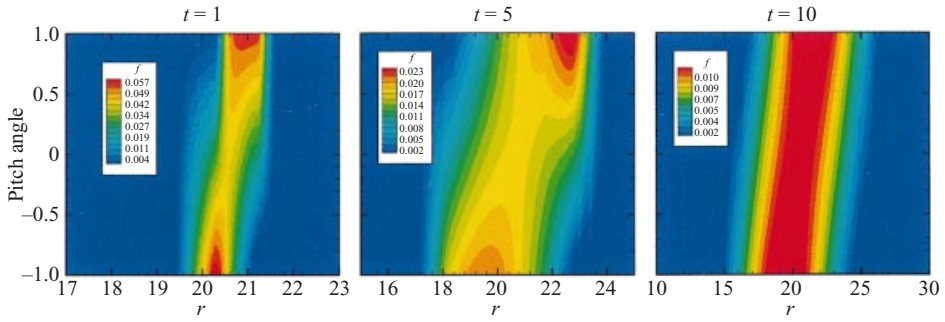

Figure 18. The particle distribution plotted as a function of position r and pitch angle μ in a time sequence $t = 1, 5, 10$. The colour refers to particle number density. Here plots are for a normalized particle velocity $v = 1.0$ and $U = 0.1$ (where U is normalized to v).

https://doi.org/10.1017/S0022377800008709 Published online by Cambridge University Press

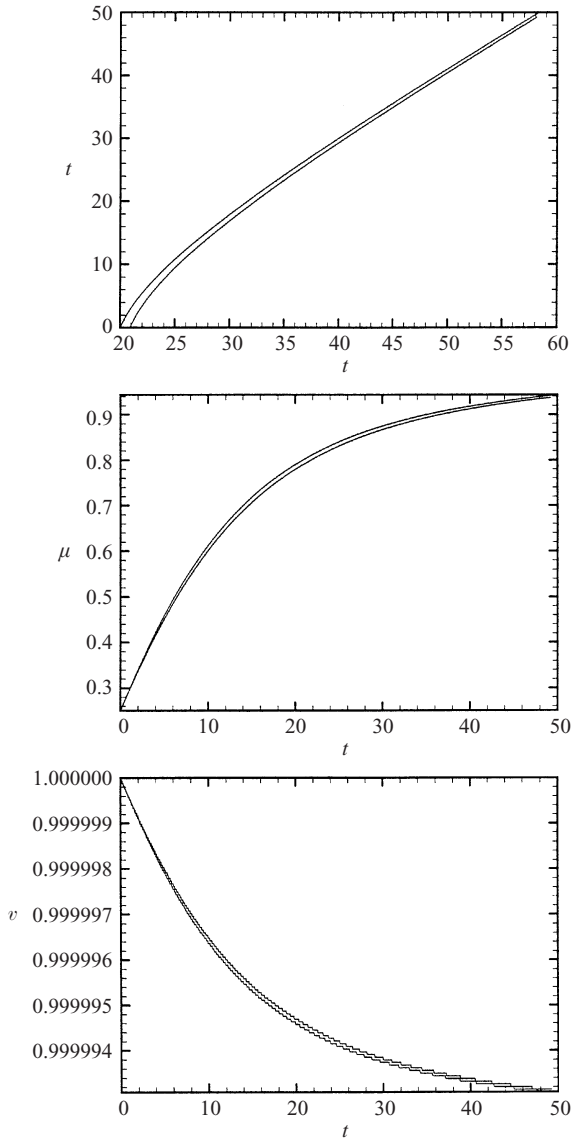

Figure 17. Unscattered-particle trajectories in the presence of adiabatic deceleration and focusing.

4.2. Adiabatic deceleration

The inclusion of the adiabatic term in (1.4) now renders the expanded equations in F and f^s more complicated, since the order of the partial differential equations is increased by one,

$$\frac{\partial F}{\partial t}+\mu v\frac{\partial F}{\partial r}-\frac{1-\mu^2}{r}uv\frac{\partial F}{\partial v}+\frac{1-\mu^2}{r}v\frac{\partial F}{\partial \mu}=-\frac{F}{\tau}, \tag{4.10}$$

$$\frac{\partial f^s}{\partial t}+\mu v\frac{\partial f^s}{\partial r}-\frac{1-\mu^2}{r}uv\frac{\partial f^s}{\partial v}+\frac{1-\mu^2}{r}v\frac{\partial f^s}{\partial \mu}=\frac{f_0-f^s}{\tau}+\frac{F_0}{\tau}, \tag{4.11}$$

https://doi.org/10.1017/S0022377800008709 Published online by Cambridge University Press

and the unscattered particles satisfy

$$F = F(r, t = 0, \mu, v)e^{-t/\tau}, \tag{4.12}$$

$$r(1-\mu^2)^{1/2} = r_0(1-\mu_0^2)^{1/2} = A_1, \tag{4.13}$$

$$\mu u + v = \mu_0 u + v_0 = A_2, \tag{4.14}$$

$$\frac{dr}{A_2\left(1-\frac{A_1^2}{r^2}\right)^{1/2} - u\left(1-\frac{A_1^2}{r^2}\right)} = dt. \tag{4.15}$$

The unscattered particle trajectories (4.12)–(4.15) are illustrated in Fig. 17. From (4.10), we obtain the infinite set of equations

$$\begin{aligned}(2n+1)\frac{\partial f_n}{\partial t} + (n+1)v\frac{\partial f_{n+1}}{\partial r} + nv\frac{\partial f_{n-1}}{\partial r} - \left[(2n+1) - \frac{(n+1)^2}{2n+3} - \frac{n^2}{2n-1}\right]\frac{uv}{r}\frac{\partial f_n}{\partial v} \\ + \frac{n(n-1)}{2n-1}\frac{uv}{r}\frac{\partial f_{n-2}}{\partial v} + \frac{(n+1)(n+2)}{2n+3}\frac{uv}{r}\frac{\partial f_{n+2}}{\partial v} + (n+2)(n+1)\frac{v}{r}f_{n+1} \\ - n(n-1)\frac{v}{r}f_{n-1} + (2n+1)\frac{f_n}{\tau} = (2n+1)\frac{\delta_{n0}}{\tau}(f_0 + F_0).\end{aligned} \tag{4.16}$$

The f_1 approximation is considerably more complicated than before, and is given by

$$\frac{\partial f_0}{\partial t} = -v\frac{\partial f_1}{\partial r} + \frac{2uv}{3r}\frac{\partial f_0}{\partial v} + \frac{F_0}{\tau} - \frac{2v}{r}f_1, \tag{4.17}$$

$$\frac{\partial f_1}{\partial t} = -\frac{v}{3}\frac{\partial f_0}{\partial r} + \frac{2uv}{5r}\frac{\partial f_1}{\partial v} - \frac{f_1}{\tau}. \tag{4.18}$$

To solve (4.17) and (4.18), we introduce an operator split and solve the resulting equations using a method of characteristics closely analogous to that used in the previous sections. Thus, we solve sequentially

$$\frac{\partial f_0}{\partial t} + v\frac{\partial f_1}{\partial r} + \frac{2v}{r}f_1 = \frac{F_0}{\tau}, \tag{4.19}$$

$$\frac{\partial f_1}{\partial t} + \frac{v}{3}\frac{\partial f_0}{\partial r} = -\frac{f_1}{\tau}. \tag{4.20}$$

and

$$\frac{\partial f_0}{\partial t} - \frac{2u}{3r}\frac{\partial f_0}{\partial \xi} = 0, \tag{4.21}$$

$$\frac{\partial f_1}{\partial t} - \frac{2u}{5r}\frac{\partial f_1}{\partial \xi} = 0, \tag{4.22}$$

where $\xi = \ln v$. Equations (4.19) and (4.20) correspond exactly to those of Sec. 4.1, with the same characteristic speeds obviously, and can be solved in precisely the same way. However, after each time step, the velocity distribution needs to be updated using (4.21) and (4.22) along each of the characteristics of the

https://doi.org/10.1017/S0022377800008709 Published online by Cambridge University Press

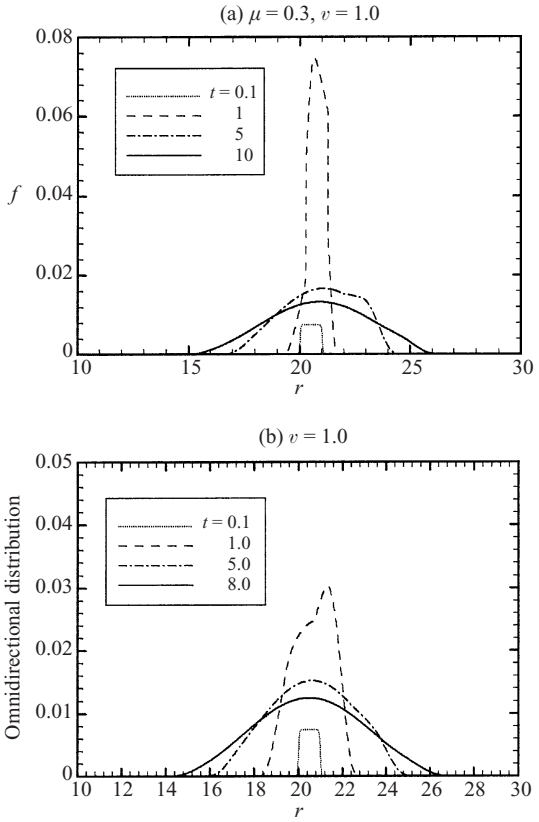

Figure 19. (a) The directional distribution f for $\mu = 0.3$ and $v = 1.0$ at four times $t = 0.1$, 1, 5, 10. (b) The omnidirectional distribution $\langle f \rangle$ for $v = 1.0$ at the same times.

hyperbolic system (4.19) and (4.20). Equations (4.21) and (4.22) are simple enough to solve analytically along each of the characteristic segments determined from (4.19) and (4.20), so that

$$r^{\pm}(t) = \pm \frac{v}{\sqrt{3}}, (t - t_n) + r_n, \tag{4.23}$$

where (t_n, r_n) refers to the preceding time step at position r_n. Thus, the particle velocity along each characteristic changes according to

$$\frac{dv}{dt} = -\frac{2u}{3} \frac{v}{\pm (v/\sqrt{3})(t - t_n) + r_n}. \tag{4.24}$$

The numerical solution of (4.15) and (4.16) is then quite straightforwardly obtained by an extension of our basic numerical scheme described in the previous sections.

Figures 18–20 illustrate solutions to (1.4) when adiabatic deceleration is included. Initially, the beams propagate to the right and left, and were located at $20 < r < 21$ and had $\mu_0 = 0.25$. Figure 18 (page 533) shows the spatial and

https://doi.org/10.1017/S0022377800008709 Published online by Cambridge University Press

pitch-angle distribution for three different normalized times. At early times $t = 1$, the distribution remains highly anisotropic. Only at later times ($t = 10$) does the distribution relax to a more spatially isotropic state. Figure 19(a) illustrates the directional distribution f for a particular μ ($= 0.3$) and v ($= 1.0$). As before, the beam is noticeable at early times but scarcely influences the solution by $t = 10$. Figure 19(b) shows the temporal evolution of the omnidirectional distribution $\langle f \rangle$. A convenient depiction of the phase space distribution function is shown in Fig. 20(a–c), where the particle number density is plotted as a function of $(v_\parallel, v_\perp)$ (with respect to the radial magnetic field). At $t = 3$, $r = 22$, the cooled particle distribution is contained primarily in the right hemisphere (compare with Fig. 18). By $t = 15$, the right hemisphere exhibits a pronounced cooling, and the distribution is more isotropic – at least in the cooled particles. Figure 20(c) corresponds to $r = 19$, $t = 15$, and illustrates that the backward-propagating ions have experienced considerable adiabatic cooling. Figure 20(d) illustrates the total directional distribution function f plotted as a function of position and time for a particular μ and particle velocity v. Plotted in this way, the scattering of the particles within the boundaries determined by the forward and backward characteristics (Sec. 2.1), as well as the cooling of the distribution in the expanding solar wind, is revealed very clearly.

5. Conclusions

Charged-particle transport in space and astrophysical plasmas is determined by magnetic fields that are ordered on a large scale but are highly stochastic on smaller scales. Fluctuating magnetic fields act to scatter charged particles in pitch angle, and their transport is governed by the Fokker–Planck equation with a scattering operator. In this paper we have considered a spherically expanding supersonic flow (nominally the solar wind) with constant velocity and radial magnetic field. We have furthermore considered only very fast particles ($v \gg u$). The scattering operator can assume a large-angle scattering form, modelled as a BGK relaxation-time operator, a small-angle scattering form derived from quasilinear theory, or a combination of both. In this paper, we restrict our attention to large-angle scattering exclusively, but the techniques developed here can be applied to the small-angle quasilinear scattering operator (Part 2).

Our goal in this series of papers is to develop a quasinumerical approach to solving the Fokker–Planck equation, in the presence of small- and of large-angle scattering, that is valid for all times t, including $t \ll \tau$, where τ is an effective scattering time. To achieve this, we use a novel 'propagating-source' method in which the particle distribution function is separated into an unscattered part and a scattered part. The unscattered particles represent the source distribution for particles that experience scattering. Accordingly, the unscattered particles decay exponentially as $F \propto \exp(-t/\tau)$. The 'decay time' of the unscattered particles derives from the scattering time scale that enters either the BGK relaxation time operator or the quasilinear scattering operator.

The decomposition of the particle distribution function into scattered and unscattered components and the resulting introduction of a propagating source for the scattered particle population proves to be a surprisingly effective

https://doi.org/10.1017/S0022377800008709 Published online by Cambridge University Press

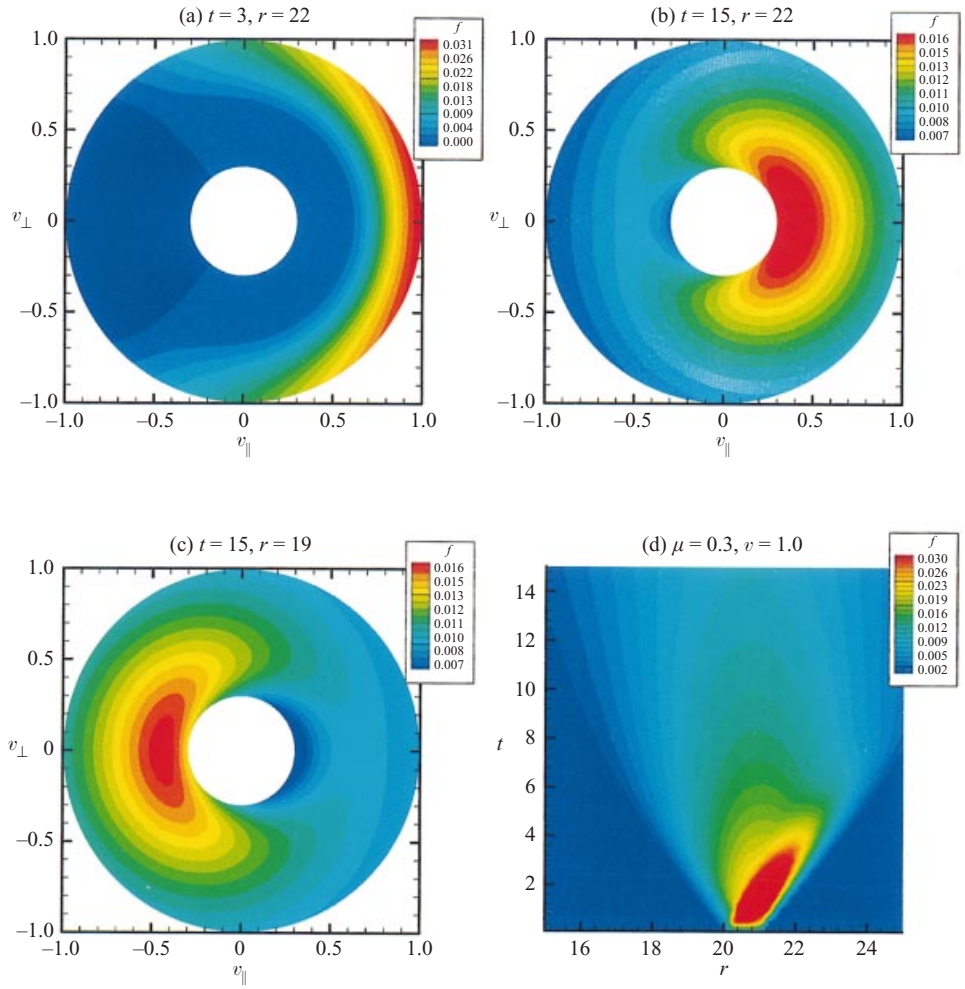

Figure 20. (a–c) Phase-space plots of the adiabatically cooled distribution function. Here $v_\parallel$ and $v_\perp$ refer to the particle velocity parallel and perpendicular to the radial magnetic field. (d) Plot of the distribution function in (r, t) space for $\mu = 0.3$ and $v = 1$. The colour refers to particle number density.

approach to capturing the so-called 'flash phase' of particle propagation, i.e. particle propagation in the time shortly after the impulsive release of particles and before the distribution has experienced much scattering. By way of example, we have reconsidered the derivation of the well-known telegrapher equation, which describes the omnidirectional phase-space density of charged particles with a fixed speed v. For simple isotropic scattering and an impulsive isotropic source, the telegrapher equation predicts the instantaneous formation of leading pulses that propagate ahead of the diffusive wake. By contrast, the propagating-source technique yields an inhomogeneous telegrapher equation for the omnidirectional distribution, which does not admit coherent pulses in the solution. Instead, a well-defined particle 'wave front' heads the 'diffusive' scattered particle population.

https://doi.org/10.1017/S0022377800008709 Published online by Cambridge University Press

In solving the transport equation for the scattered particles, we draw on polynomial expansion methods. We have shown that the truncation of the infinite system of equations derived from the harmonics of the polynomial expansion of the Boltzmann equation forms a linear hyperbolic system of partial differential equations. The characteristic speeds of the nth-order truncation correspond to the 'speeds' into which the particles are scattered. In particular, for isotropic scattering models, we have shown that even-order truncations are inherently more accurate than odd-order truncations of the polynomial-expanded Boltzmann equation. This is a consequence of the even-order truncations admitting $\frac{1}{2}n$ forward-propagating and $\frac{1}{2}n$ backward-propagating characteristics and a single stationary characteristic. For the odd-order truncations, the stationary characteristic is always absent, and, as a result, the odd-order truncations – no matter how refined or high-order – can never capture accurately particle propagation for particles with pitch angles close to zero i.e. nearly stationary scattered particles. Since increasing the truncation order increases the number of characteristic speeds into which the particle distribution can be scattered, a higher-order truncation increases the accuracy of the solution. However, provided that we use an even-order truncation, we find that low-order polynomial expansions prove remarkably accurate, with, for example, an f_2 approximation giving almost identical results to a higher-order f_4 approximation. This, however, is true only if the propagating-source method is utilized.

Since the truncated Boltzmann equation reduced to a system of linear hyperbolic equations, the very powerful and accurate numerical method of characteristics is ideally suited to solving the equations. This has proved relatively straightforward to implement, and has yielded accurate results. The inclusion of adiabatic deceleration terms necessitated the introduction of an operator split into the numerical characteristic scheme. The split equations are solved along elements of the characteristics.

In view of our decomposition of the particle distribution, the moving-source technique lends itself to the investigation of arbitrarily anisotropic initial data. Example solutions have been computed using different ring-beam distributions. The ability of this numerical method to consider non-isotropic initial data represents a decided advantage over other approaches. As we shall discuss in Part 2, the numerical scheme developed here is equally useful for the case of a small-angle quasilinear scattering operator.

A further application of the propagating-source technique discussed here has been to solve the Boltzmann equation in the presence of an anisotropic scattering operator. This corresponds to a model introduced by Kota (1994). Comparison of our low-order polynomial-expansion solution to the exact solutions obtained by Kota has demonstrated the accuracy of the numerical scheme, and supports the use of a low-order truncation. The additional inclusion of focusing and adiabatic deceleration to the Boltzmann equation has also been addressed, and the propagating-source technique has readily been extended to these more complicated problems.

A comprehensive investigation of the various solutions to the BGK Boltzmann equation has also been presented. An understanding of charged-particle transport is of particular importance in the solar wind. Very energetic charged-particle populations are frequently released impulsively at the Sun

during periods of great solar activity (flares, etc.). These populations stream along the ambient IMF, experiencing scattering, and are observed at 1 AU by spacecraft or, if energetic enough, by neutron monitors. The relative importance of effects such as focusing, adiabatic deceleration, and scattering in determining the characteristics of the observed energetic particles is not easily disentangled. Our analysis of the different limits of the BGK Boltzmann equation therefore sheds considerable light on our understanding of episodic energetic particle populations observed at the Earth. A detailed discussion of the results for the various models can be found in the appropriate sections above, and is not repeated here. There is, however, one overriding conclusion to emerge from this study, which is that particle beams that experience scattering by interplanetary fluctuations are likely to remain highly anisotropic for many scattering times. This makes the use of the diffusion approximation for charged-particle transport particularly dangerous under many reasonable solar-wind conditions, especially in the inner heliosphere.

Acknowledgements

The partial support of NASA Grant NAG5-7796, a University of Delaware NASA Space Grant College Award, and NSF Grants ATM-0072810 and ATM-9713432 is acknowledged. G.M.W. acknowledges the support of NASA Grant NAG5-5180.

References

Burlaga, L. F. 1995 *Interplanetary Magnetohydrodynamics*. Oxford University Press.

Chalov, S. V. and Fahr, H. J. 1998 *Astron. Astrophys.* **335**, 746.

Chalov, S. V. and Fahr, H. J. 1999a *Astrophys. Space Sci.* **264**, 509.

Chalov, S. V. and Fahr, H. J. 1999b *Solar Phys.* **187**, 123.

Dougherty, J. P., Watson, S. R. and Hellberg, M. A. 1967 *J. Plasma Phys.* **1**, 327.

Earl, J. A. 1974 *Astrophys. J.* **188**, 379.

Earl, J. A. 1993 In: *Proceedings of 23rd International Cosmic Ray Conference*, Vol. 3, p. 360.

Earl, J. A. 1995 In: *Proceedings of 24th International Cosmic Ray Conference*, Vol. 4, p. 293.

Fedorov, Yu I. and Shakhov, B. A. 1993 In: *Proceedings of 23rd International Cosmic Ray Conference*, Vol. 3, p. 215.

Fedorov, Yu I., Shakhov, B. A. and Stehlik, M. 1995 *Astron. Astrophys.* **302**, 623.

Fisk, L. A. and Axford, W. I. 1969 *Solar Phys.* **7**, 46.

Fisk, L. A., Schwadron, N. A. and Gloeckler, G. 1997 *Geophys. Res. Lett.* **24**, 93.

Gleeson, L. J. and Axford, W. I. 1967 *Astrophys. J.* **149**, L115.

Gloeckler, G. and Geiss, J. 1998 *Space Sci. Rev.* **86**, 127.

Gombosi. T. I., Jokipii, J. R., Kota, J., Lorencz, K. and Williams, L. L. 1993 *Astrophys. J.* **403**, 377.

Hasselmann, K. and Wibberenz, G. 1970 *Astrophys. J.* **162**, 1049.

Heras, A. M., Sanahuja, B., Lario, D., Smith, Z. K., Detman, T. and Dryer, M. 1995 *Astrophys. J.* **445**, 497.

Isenberg, P. A. 1997 *J. Geophys. Res.* **102**, 4719.

Jokipii, J. R. 1966 *Astrophys. J.* **146**, 480.

Kallenrode, M.-B. and Hatzky, R. 1999 In: *Proceedings of 26th International Cosmic Ray Conference*, Vol. 6, p. 324.

Kota, J. 1994 *Astrophys. J.* **427**, 1035.

Kota, J., Merenyi, E., Jokipii, J. R., Kopriva, D. A., Gombosi, T. I. and Owens, A. J. 1982 *Astrophys. J.* **254**, 398.

Lu, J. Y. and Zank, G. P. 2000 *J. Geophys. Res* (in press).

Ng, C. K. and Wong, K.-Y. 1979 In: *Proceedings of 16th International Cosmic Ray Conference*, Vol. 5, p. 252.

Pauls, L. H. and Burger, R. A. 1993 In: *Proceedings of 23rd International Cosmic Ray Conference*, Vol. 3, p. 191.

Ruffolo, D. 1991 *Astrophys. J.* **382**, 688.

Ruffolo, D. and Khumlumlert, T. 1995 *Geophys. Res. Lett.* **22**, 2073.

Schwadron, N. A. 1998 *J. Geophys. Res.* **103**, 20643.

Schwadron, N. A. and Gombosi, T. I. 1994 *J. Geophys. Res.* **9**, 19301.

Skilling, J. 1971 *Astrophys. J.* **170**, 265.

Webb, G. M., Zank, G. P., Pantazopoulou, M. and Zakharian, A. K. 1999 In: *Proceedings of 26th International Cosmic Ray Conference*, Vol. 6, p. 351.

Webb, G. M., Pantazopoulou, M. and Zank, G. P. 2000 *J. Phys. A: Math. Gen.* **33**, 3137.

Zank, G. P., Lu, J. Y., Dröge, W. and Bieber, J. W. 2000 Transport of energetic charged particles in a radial magnetic field. Part 2. Small-angle scattering. Manuscript in preparation.

Zank, G. P., Matthaeus, W. H., Bieber, J. W. and Moraal, H. 1998 *J. Geophys. Res.* **103**, 2085.

Zank, G. P., Lu, J. Y., Rice, W. K. M. and Webb, G. M. 1999 In: *Proceedings of 26th International Cosmic Ray Conference*, Vol. 6, p. 312.